Methane, carbon dioxide, and nitrous oxide emissions from two clear-water and two turbid-water urban ponds in Brussels (Belgium)

Thomas Bauduin [1,2], Nathalie Gypens [1], Alberto V. Borges [2]

[1]Ecology of Aquatic Systems, Université Libre de Bruxelles, Belgium
[2]Chemical Oceanography Unit, University of Liège, Belgium

Correspondence to: Alberto V. Borges (alberto.borges@uliege.be)

Abstract. Shallow ponds can occur either in a clear-water state dominated by macrophytes or a turbid-water state dominated by phytoplankton, but it is unclear if and how these two alternative states affect the emission of greenhouse gases (GHGs) such as carbon dioxide (CO_2), methane (CH_4), and nitrous oxide (N_2O) to the atmosphere. We measured the dissolved concentration of CO_2, CH_4, and N_2O from which the diffusive air-water fluxes were computed, in four urban ponds in the city of Brussels (Belgium): two clear-water macrophyte-dominated ponds (Silex and Tenreuken), and two turbid-water phytoplankton-dominated ponds (Leybeek and Pêcheries) on 46 occasions over 2.5 years (between June 2021 and December 2023). Ebullitive CH_4 fluxes were measured with bubble traps in the four ponds during deployments in spring, summer, and fall, totalling 48 days of measurements. Measured ancillary variables included water temperature, oxygen saturation level ($\%O_2$), concentrations of chlorophyll-*a* (Chl-*a*), total suspended matter (TSM), soluble reactive phosphorus (SRP), nitrite (NO_2^-), nitrate (NO_3^-), and ammonium (NH_4^+). The turbid-water and clear-water ponds did not differ significantly in terms of diffusive emissions of CO_2 and N_2O. Clear-water ponds exhibited higher values of ebullitive CH_4 emissions compared to turbid-water ponds, most probably in relation to the delivery of organic matter from macrophytes to sediments, but the diffusive CH_4 emissions were not significantly different between clear- and turbid-water ponds. Across seasons, CH_4 emissions increased with water temperature in all four ponds, with ebullitive CH_4 fluxes having a stronger dependence on water temperature (Q_{10}) than diffusive CH_4 fluxes. The temperature sensitivity of ebullitive CH_4 fluxes decreased with increasing water depth, implying that shallow sediments would respond more strongly to warming (*e.g.* heat waves). Total annual CH_4 emissions (diffusive+ebullitive) in CO_2 equivalents equalled those of CO_2 in turbid-water ponds and exceeded those of CO_2 in clear-water ponds, while N_2O emissions were negligible compared to the other two GHGs. Total annual GHG emissions in CO_2 equivalents from all four ponds increased from 2022 to 2023 due to higher CO_2 diffusive fluxes, likely driven by higher annual precipitation in 2023 compared to 2022 (leading putatively to higher inputs for organic or inorganic carbon from run-off), possibly in response to the intense El Niño event of 2023. The findings of this work suggest that it might be necessary to account for the presence of submerged macrophytes when extrapolating ebullitive CH_4 fluxes in ponds at larger scale (regional or global) (particularly if Chl-*a* is used as a descriptor), although it might be less critical for the extrapolation of diffusive CH_4, CO_2, and N_2O fluxes.

1. Introduction

Greenhouse gas (GHG) emissions from inland water (rivers, lakes, and reservoirs) to the atmosphere such as carbon dioxide (CO_2), methane (CH_4), and nitrous oxide (N_2O) are quantitatively important for global budgets (Lauerwald et al., 2023). Global GHG emissions from lakes are lower than from rivers for CO_2 (Raymond et al., 2013) and for N_2O (Lauerwald et al., 2019; Maavara et al., 2019). However, reported global emissions of CH_4 from lakes (Rosentreter et al., 2021; Johnson et al., 2022) are equivalent or even higher compared to rivers (Stanley et al., 2016; Rocher-Ros et al., 2023). Global emissions of

CO_2 and CH_4 from lakes to the atmosphere represent 1.25 to 2.30 Pg CO_2 equivalents (CO_2-eq) annually with a significant proportion from CH_4 emissions, and represent nearly 20% of global CO_2 emissions from fossil fuels (Delsontro et al., 2018). The contribution of CO_2 and CH_4 emissions from small lentic water bodies (small lakes and ponds) can be disproportionately high compared to large systems (Holgerson and Raymond, 2016) as small lakes and ponds are the most abundant of all water body types in number (Verpoorter et al., 2014; Cael et al., 2017), and fluxes per m^2 are usually higher from smaller water bodies. The emissions of GHGs from artificial water bodies such as agricultural reservoirs, urban ponds, and storm-water retention basins could be higher than those from natural systems (Martinez-Cruz et al., 2017; Grinham et al., 2018; Herrero Ortega et al., 2019; Gorsky et al., 2019; Ollivier et al., 2019; Peacock et al., 2019, 2021; Webb et al., 2019; Bauduin et al., 2024). These higher GHG emissions seem to result from higher external inputs of anthropogenic organic carbon and dissolved inorganic nitrogen (DIN) into artificial systems, but might also reflect other differences compared to natural systems such as in hydrology (Clifford and Heffernan, 2018). Among artificial systems, urban ponds are the subject of a growing body of literature on GHG emissions (Singh et al., 2000; Natchimuthu et al., 2014; van Bergen et al., 2019; Audet et al., 2020; Peacock et al., 2021; Goeckner et al., 2022; Ray and Holgerson, 2023; Ray et al. 2023; Bauduin et al., 2024). Urban areas can have numerous small artificial water bodies mostly associated to green spaces such as public parks, and their number is increasing due to rapid urbanisation worldwide (Brans et al., 2018; Audet et al., 2020; Gorsky et al., 2024; Rabaey et al., 2024). Urban ponds are generally small, shallow, and usually their catchment consists in majority of impervious surfaces with a smaller contribution from soils (Davidson et al., 2015; Peacock et al., 2021). In general, the main function of urban ponds is for storm-water management but they provide additional benefits including aesthetic/recreational amenities and habitats for wildlife (e.g. Tixier et al., 2011; Hassall, 2014).

Shallow ponds and lakes occur in two alternative states corresponding to systems with either clear waters (macrophyte-dominated) or turbid waters (phytoplankton-dominated), during the productive period of the year (spring and summer in mid-latitudes) (Scheffer et al., 1993). Submerged macrophytes and phytoplankton regulate CO_2 dynamics directly through photosynthesis that can be more or less balanced by community respiration in the water column (*e.g.*, Sand-Jensen and Staehr, 2007). However, it is not clear whether the presence of macrophytes increases or decreases the net CO_2 emissions from ponds and lakes. Some studies have shown a decrease of CO_2 emissions with increasing macrophyte density (Kosten et al., 2010; Ojala et al., 2011; Davidson et al., 2015), but other studies showed the opposite pattern (Theus et al., 2023). In phytoplankton-dominated lakes, CO_2 concentrations depend in part on the developmental stage of phytoplankton, with the growth and peak phases generally coinciding with lower CO_2 concentrations due to photosynthesis (Grasset et al., 2020; Vachon et al., 2020).

CH_4 emissions have been reported to increase with the concentration of chlorophyll-*a* (Chl-*a*) in phytoplankton-dominated lakes (DelSontro et al., 2018; Borges et al., 2022). The presence of macrophytes strongly affects the production of CH_4 in freshwaters (Bastviken et al., 2023) and vegetated littoral zones of lakes exhibit higher CH_4 emissions than non-vegetated zones (Hyvönen et al., 1998; Huttunen et al., 2003; Juutinen et al., 2003; Desrosiers et al., 2022; Theus et al., 2023). Macrophytes influence organic matter decomposition processes in sediments depending on the quality and quantity of plant matter they release into their environment (Reitsema et al., 2018; Grasset et al., 2019; Harpenslager et al., 2022; Theus et al., 2023). Yet, few studies have consistently compared CH_4 emissions in clear-water and turbid-water ponds (Hilt et al., 2017). A study in Argentina reported higher dissolved CH_4 concentrations in clear-water ponds with submerged macrophytes compared to turbid-water phytoplankton-dominated ponds, but no differences in measured CH_4 emissions (Baliña et al., 2023).

The production of N_2O predominantly occurs through microbial nitrification and denitrification that depend on DIN, O_2 levels, and temperature (Codispoti and Christensen, 1985; Mengis et al., 1997; Velthuis and Veraart, 2022). Competition for DIN between primary producers and N_2O-producing microorganisms can impact N_2O production. Additionally, the transfer of labile phytoplankton organic matter to sediments fuels benthic denitrification and impacts N_2O fluxes. Eutrophication is assumed to drive high N_2O emissions from lakes and ponds (Audet et al., 2020; Webb et al., 2021; Wang et al., 2021; Xie et al., 2024) but some lakes with elevated Chl-*a* concentrations can act as sinks of N_2O due to removal of N_2O by denitrification (Webb et al., 2019; Borges et al., 2022; 2023). The presence of macrophytes also strongly influences nitrogen cycling in sediments of lakes and ponds (Barko et al., 1991; Choudhury et al., 2018; Deng et al., 2020; Dan et al., 2021) and should in theory also affect N_2O emissions, although seldom investigated, and available studies provide contradictory conclusions. N_2O emissions have been shown to follow diurnal cycles of O_2 concentrations in areas dominated by submerged macrophytes in Lake Wuliangsuhai (China) (Ni et al., 2022) and the seasonal cycle of aboveground biomass of emerged macrophytes (*Phragmites*) in Baiyangdian Lake (China) (Yang et al., 2012). On the contrary, a study showed there was no significant difference of N_2O production in sediments of macrophyte-rich (n=10) and macrophyte-free (n=12) lakes in subtropical China (Liu et al., 2018). There has been a very limited number of studies systematically investigating how emissions differ between ponds dominated by phytoplankton and those dominated by macrophytes (Baliña et al., 2023), and none investigating simultaneously CO_2, CH_4, and N_2O emissions including both diffusive and ebullitive components.

The emissions of CO_2 and N_2O from aquatic systems are exclusively through diffusion across the air-water interface (diffusive flux), while CH_4 can be additionally emitted as bubbles released from sediments to the atmosphere (ebullitive flux). At annual scale, ebullitive CH_4 flux usually represents more than half of total (diffusive+ebullitive) CH_4 emissions from shallow lakes (Wik et al., 2013; Deemer and Holgerson, 2021), although the relative contribution of ebullitive and diffusive CH_4 emissions is highly variable seasonally (*e.g.* Wik et al., 2013; Ray and Holgerson, 2023; Rabaey and Cotner 2024). Ebullitive CH_4 fluxes are particularly high in the littoral zone of lakes at depths <5 m (Wik et al., 2013; DelSontro et al., 2016; Borges et al., 2022) and strongly increase in response to temperature (DelSontro et al., 2016; Aben et al., 2017; Rabaey and Cotner 2024), as well as organic matter availability (DelSontro et al., 2016; 2018). Ebullitive CH_4 fluxes tend to be higher in small and shallow water bodies (Deemer and Holgerson, 2021) but are notoriously variable in time and space, and are difficult to estimate reliably (DelSontro et al., 2011).

Here, we report a dataset of CO_2, CH_4, and N_2O dissolved concentrations in four shallow and small urban ponds (Leybeek, Pêcheries, Silex, and Tenreuken) in the city of Brussels (Belgium) (Fig. 1), with data collected 46 times at regular intervals (between June 2021 and December 2023) on each pond. The air-water diffusive fluxes of CO_2, CH_4, and N_2O were calculated from dissolved concentrations and the gas transfer velocity, while the ebullitive CH_4 fluxes were measured with inverted funnels during 8 deployments (totalling 48 days) in the four ponds. The four ponds have similar depth, surface area, and catchment urban coverage, and mainly differ by the phytoplankton-macrophyte dominance, a clear-water state dominated by macrophytes and a turbid-water state dominated by phytoplankton (alternative states) (Fig. 1). We assess whether the differences in terms of (i) CO_2, CH_4, and N_2O dissolved concentration and diffusive emissions; (ii) ebullitive CH_4 emissions; (iii) relative contribution of CO_2, CH_4, and N_2O to the total GHG emissions in CO_2-eq between the four ponds are explained by the two alternative states.

2. Material and Methods

2.1. Field sampling and meteorological data

Sampling was carried out at a single fixed station (pontoon) in each of the four ponds, on the same day between 9am and 11am, 46 times on each pond between June 2021 and December 2023 at a frequency ranging from one (winter) to three (summer) times per month. Water was sampled 5 cm below the surface with 60 ml polypropylene syringes for analysis of dissolved concentrations of CO_2, CH_4, and N_2O. Samples for CH_4 and N_2O were transferred from the syringes with a silicone tube into 60 ml borosilicate serum bottles (Wheaton), preserved with 200 µl of a saturated solution of $HgCl_2$, sealed with a butyl stopper and crimped with aluminium cap, without a headspace, and stored at ambient temperature in the dark prior to analysis in the laboratory. The partial pressure of CO_2 (pCO_2) was measured directly in the field, within 5 minutes of sample collection, with a Li-Cor Li-840 infrared gas analyser (IRGA) based on the headspace technique with 4 polypropylene syringes (Borges et al., 2019). A volume of 30 ml of sample water was equilibrated with 30 ml of atmospheric air within the syringe by shaking vigorously for 5 minutes. The headspace of each syringe was then sequentially injected into the IRGA and a fifth syringe was used to measure atmospheric CO_2. The final pCO_2 value was computed taking into account the partitioning of CO_2 between water and the headspace, as well as equilibrium with HCO_3^- (Dickson et al., 2007) using water temperature measured in-situ and after equilibration, and total alkalinity (data not shown). Samples for total alkalinity were conditioned, stored, and analysed as described by Borges et al. (2019). The IRGA was calibrated in the laboratory with ultrapure N_2 and a suite of gas standards (Air Liquide Belgium) with CO_2 mixing ratios of 388, 813, 3788 and 8300 ppm. The precision of pCO_2 measurements was ±2.0%. Water temperature, specific conductivity, and oxygen saturation level ($\%O_2$) were measured in-situ with VWR MU 6100H probe 5 cm below the surface. A 2 liter polyethylene water container was filled with surface water for conditioning the samples for other variables at the laboratory in Université Libre de Bruxelles.

Three bubble traps were deployed 50 cm apart for measuring ebullitive CH_4 flux. The bubble traps consisted of inverted polypropylene funnels (diameter 23.5 cm) mounted with 60 ml polypropylene syringes, with three way stop valves allowing to collect the gas without contamination from ambient air. The polypropylene funnel was attached with steel rods to a polystyrene float. The volume of gas collected in the funnels was sampled with graduated polypropylene 60 ml syringes every 24 hours. The value of the collected volume of gas was logged, and the gas was transferred immediately after collection to pre-evacuated 12 ml vials (Exetainers, Labco, UK) that were stored at ambient temperature in the dark prior to the analysis of CH_4 concentration in the laboratory. The time-series of measurements was longer at the Silex pond than the other three ponds.

Surveys to identify and quantify visually the relative coverage of emerged and submerged macrophytes were conducted in summer 2023 (Table S1). The resulting list of macrophyte species agreed with past studies in Brussels' ponds (Peretyatko et al., 2007). Air temperature, precipitation, wind speed, and atmospheric pressure, were retrieved from https://wow.meteo.be/en for the meteorological station of the Royal Meteorological Institute of St-Lambert (50.8408°N, 4.4234°E) in Brussels, located between 2.5 and 5.0 km from the surveyed ponds. Air temperature, wind speed and atmospheric pressure were averaged over 24 h to obtain a daily mean value. Precipitation was integrated each day to obtain cumulated daily value.

2.2. Laboratory analysis

2.2.1. Chlorophyll-*a*, total suspended matter, and dissolved inorganic nutrients

Water was filtered through Whatman GF/F glass microfiber filters (porosity 0.7 µm) with a diameter of 47 mm for total suspended matter (TSM) and Chl-*a*. Filters for TSM were dried in an oven at 50 °C and filters for Chl-*a* were kept frozen (-20 °C). The weight of each filter was determined before and after filtration of a known volume of water using an Explorer™ Pro EP214C analytical microbalance (accuracy ±0.1 mg) for determination of TSM concentration. Chl-*a* concentration was measured on extracts with 90% acetone by fluorimetry (Kontron model SFM 25) (Yentsch and Menzel, 1963) with a limit of detection of 0.01 µg L^{-1}. Filtered water was stored frozen (-20 °C) in 50 ml polypropylene bottles for analysis of dissolved nutrients. Soluble reactive phosphorus (SRP) was determined by the ammonium molybdate, ascorbic acid and potassium antimony tartrate staining method (Koroleff, 1983), with a limit of detection of 0.1 µmol L^{-1}. Ammonium (NH_4^+) was determined by the nitroprusside-hypochlorite-phenol staining method (Grasshoff and Johannsen, 1972), with a limit of detection of 0.05 µmol L^{-1}. Nitrite (NO_2^-) and nitrate (NO_3^-) were determined before and after reduction of NO_3^- to NO_2^- by a cadmium-copper column, using the Griess acid reagent staining method (Grasshoff et al., 2009), with a detection limit of 0.01 and 0.1 µmol L^{-1}, respectively. Concentration of dissolved inorganic nitrogen (DIN) was calculated as the sum of NH_4^+, NO_2^- and NO_3^- concentrations in µmol L^{-1}.

2.2.2. CH_4 and N_2O measurements by gas chromatography

Measurements of N_2O and CH_4 concentrations dissolved in water were made with the headspace technique (Weiss, 1981) with an headspace volume of 20 ml of ultra-pure N_2 (Air Liquid Belgium) and a gas chromatograph (GC) (SRI 8610C) with a flame ionisation detector for CH_4 and an electron capture detector for N_2O calibrated with CH_4:N_2O:N_2 gas mixtures (Air Liquide Belgium) with mixing ratios of 1, 10 and 30 ppm for CH_4, and 0.2, 2.0 and 6.0 ppm for N_2O. The precision of measurement based on duplicate samples was ±3.9% for CH_4 and ±3.2% for N_2O. Measurements of CH_4 concentration in the gas samples from bubble traps were also made by GC with the same set-up and calibration as for the determination of the dissolved concentrations in water samples.

The CO_2 concentration is expressed as partial pressure (pCO_2) in parts per million (ppm) and CH_4 as dissolved concentration (nmol L^{-1}), as frequently used in topical literature. CH_4 concentration were systematically and distinctly above saturation level (2-3 nmol L^{-1}) and pCO_2 values were below saturation only five times out of the 187 measurements. The N_2O concentrations fluctuated around atmospheric equilibrium, so data are presented as percent of saturation level (%N_2O, where atmospheric equilibrium corresponds to 100%). The equilibrium with atmosphere for N_2O was calculated from the average air mixing ratios of N_2O provided by the Global Monitoring Division (GMD) of the National Oceanic and Atmospheric Administration (NOAA) Earth System Research Laboratory (ESRL) (Dutton and Hall, 2023), and using the Henry's constant given by Weiss and Price (1980).

2.3. Calculations

2.3.1. Diffusive GHG emissions

The diffusive air-water CO_2, CH_4, or N_2O fluxes (F_G) were computed according to:

$$F_G = k \times \Delta[G] , \quad (1)$$

where k is the gas transfer velocity and Δ[G] is the air-water gas concentration gradient.

The atmospheric pCO_2 was measured in the field with the Li-Cor Li-840. For CH_4, the global average present day atmospheric mixing ratio of 1.9 ppm was used (Lan et al., 2024). k was computed from a value normalized to a Schmidt number of 600 (k_{600}) and from the Schmidt number of CO_2, CH_4 and N_2O in freshwater according to the algorithms as function of water temperature given by Wanninkhof (1992). k_{600} was calculated from the parameterization as a function of wind speed of Cole and Caraco (1998). CH_4 and N_2O emissions were converted into CO_2 equivalents (CO_2-eq) considering a 100-year timeframe, using global warming potentials of 32 and 298 for CH_4 and N_2O, respectively (Myrhe et al., 2013).

2.3.2. Ebullitive flux

Bubble flux (ml m^{-2} d^{-1}) was calculated according to:

$$F_{bubble} = \frac{V_g}{A \times \Delta t}\,, \quad (2)$$

where V_g is the volume of gas collected in the inverted funnel (ml), A is the cross-sectional surface area of the funnel (m^2), and Δt is the collection time (d).

A multiple linear regression model of F_{bubble} dependent on water temperature (T_w in °C) and drops of atmospheric pressure (Δp in atm) was fitted to the data according to:

$$\log_{10}(F_{bubble}) = \alpha \times T_w + \beta \times \Delta p + \gamma\,, \quad (3)$$

where γ is the y-intercept, α and β are the slope coefficients of the multiple linear regression model.

Δp was calculated according to Zhao et al. (2017):

$$\Delta p = -\frac{1}{\Delta t}\int_0^t p - p_0 \;\; ; \;\; \forall\; p < p_0\,, \quad (4)$$

where p is the atmospheric pressure (atm), p_0 a threshold value fixed at 1 atm, and Δt the time interval between two measurements (d) (Fig. S1).

A linear regression model of F_{bubble} dependent on T_w alone was fitted to the data according to:

$$\log_{10}(F_{bubble}) = \alpha' \times T_w + \gamma'\,, \quad (5)$$

where α' is the slope coefficient and γ' is the y-intercept.

To evaluate the relative importance of T_w and Δp combined and T_w alone in driving F_{bubble}, the values modelled based on Equations (3) and (5) were compared to the observations in the Silex pond alone or in all four ponds together, for three T_w ranges (T_w< 15°C, T_w> 15°C, and the full $T_w$range).

Ebullitive CH_4 fluxes (E_{CH4} in mmol m^{-2} d^{-1}) were calculated according to:

$$E_{CH4} = [CH_4] \times F_{bubble}\,, \quad (6)$$

where $[CH_4]$ is the measured CH_4 concentration in bubbles (mmol ml^{-1}).

The CH_4 content in bubbles expressed in % of total gas (%CH_4) was fitted with a linear regression model dependent on T_W in the Silex pond. The correlation of %CH_4 with F_{bubble} was tested on the merged data of all the four ponds.

A linear regression model of E_{CH4} dependent on T_w was fitted to the data according to:

$$\log_{10}(E_{CH4}) = b \times T_w + c \,, \quad (7)$$

where *b* is the slope and c is the y-intercept of the linear regression.

Equation (7) is used to predict E_{CH4} in each pond from measured time-series of T_W allowing matching to each diffusive CH_4 flux estimate derived from Equation (1).

The ratio of ebullitive CH_4 flux to total (diffusive + ebullitive) CH_4 flux ($\frac{Ebul}{Tot}$) was fitted as a function of T_W according to DelSontro et al. (2016):

$$\frac{Ebul}{Tot} = \frac{1}{1+f\times e^{g\cdot Tw}} \quad (8)$$

The methane ebullition Q_{10} represents the change in E_{CH4} per 10°C change in T_W and was computed according to DelSontro et al. (2016):

$$Q_{10} = 10^{10b} \,, \quad (9)$$

where *b* is given by Equation (7)

The Q_{10} of diffusive CH_4 fluxes was also computed from equation (9) but using the *b* value derived by replacing E_{CH4} by the diffusive CH_4 flux in equation (7).

2.4. Statistical analysis

Generalized linear mixed models (GLMMs) were used (1) to find differences in variables among ponds and (2) to relate GHG variables to their putative controls across all ponds and within individual ponds. GLMMs were computed with the *lme4* package (Bates et al., 2015) in R version 4.4.1 (R Core Team, 2021).

GLMMs allowed to compare pCO_2, dissolved CH_4 concentration, %N_2O, F_{bubble}, %CH_4 in bubbles, E_{CH4}, and diffusive CH_4 fluxes among the four ponds, using "sampling date" as a random effect and post-hoc tests were performed using estimated marginal means (*emmeans* package in R) to assess pairwise differences between ponds. This analysis aimed at investigating if patterns in GHG concentrations and emissions differed among ponds, in particular with regards to clear-water and turbid-water states. Data were also compared among the four ponds separated by seasons, but GLMMs did not converge due to insufficient number of data points. Comparisons on $\log_{10}$-transformed data were then made using repeated measures analysis of variance (ANOVA) (*ezANOVA* package in R) with Tukey's honestly significant difference (HSD) post-hoc tests. This analysis aimed at investigating if patterns in data shown by the data analysis with the full data-set (four seasons merged) were also observed when analyzing the data separated by seasons.

For the data-sets covering the whole sampling period (four seasons merged), GLMMs were constructed for pCO_2, dissolved CH_4 concentration, %N_2O, F_{bubble}, %CH_4 in bubbles, E_{CH4}, and diffusive CH_4 fluxes that included T_W, precipitation, %O_2,

Chl-*a*, TSM, DIN, SRP as fixed effects, and "pond" and "sampling date" as a random effect to account for repeated measurements with the *lme4* package in R. This analysis aimed at investigating (1) the impact of photosynthesis-respiration on CO_2 concentrations and emissions based the relationships with Chl-*a*, DIN, SRP; (2) the impact of the response of methanogenesis to warming on CH_4 concentrations and diffusive and ebullitive emissions based on the relationships to T_W; (3) the impact on DIN availability and T_W on N_2O concentrations and diffusive emissions. A linear regression model was used to assess the relationship between Chl-*a*, TSM, $\%O_2$, SRP, and DIN versus T_W. This analysis aimed at investigating if some of the patterns between GHG variables versus Chl-*a*, TSM, $\%O_2$, SRP, and DIN might in fact have reflected indirectly a relation between these variables and T_W. The relationships between the annual means of CH_4, CO_2 and N_2O fluxes and the annual means of a subset of variables (Chl-*a*, macrophyte cover, pond surface area and depth) were assessed with linear or quadratic regressions. The modelled F_{bubble} in the Silex pond and in the four ponds were compared to measured F_{bubble} values with a linear regression in order to evaluate the model performance. A correlation analysis was used to assess the relationship between $\%CH_4$ and F_{bubble}, as well as between anomalies in annual air temperature and annual precipitation.

The linear regression model and the Pearson correlation coefficient (r) were computed in R using the functions *lm* and *cor(method = "pearson")*, respectively. Statistical significance was set at $p<0.05$ for all analyses. Significant differences between groups presented in boxplots are indicated by lower-case letters in the Figures.

3. Results

3.1. Seasonal variations of meteorological conditions and GHG concentrations

The city of Brussels experiences a temperate climate with mild weather year-round, and evenly distributed abundant precipitation totalling on average 837 mm annually for the reference period 1991-2020. The average annual air temperature was 11 °C, with summer average of 17.9 °C and winter average of 4.1 °C for the reference period 1991-2020. During the sampling period, from June 2021 to December 2023, T_W in the surface of the four sampled ponds (Leybeek, Pêcheries, Silex, and Tenreuken; Fig. 1) tracked closely the air temperature that ranged between -1.5 and 30.0°C following the typical seasonal cycle at mid-latitudes in the Northern Hemisphere (Fig. S2). Years 2022 and 2023 were about 1 °C warmer than the average for the period 1991-2020 (11 °C), while year 2021 was closer to the long-term average (Fig. 2). Year 2022 was warmer and drier than 2021 and 2023 (Fig. 2), with positive air temperature anomalies observed evenly throughout the year (9 months out of 12) and negative precipitation anomalies in summer, fall, and early winter (Fig. S2). Year 2021 had warmer and drier months in June and September, colder and wetter months in July and August, and was overall wetter and colder than 2022 (Fig. 2). Year 2023 was marked by both positive air temperature and precipitation anomalies (Fig. S2), resulting in a wetter and warmer year than normal and compared to 2021 and 2022 (Fig. 2). Daily wind speed was generally low (<1 m s^{-1}) except for a windier period in spring 2022 (up to 5.8 m s^{-1}, corresponding to the Eunice storm) and in fall 2023 (up to 9.7 m s^{-1}, corresponding to the Ciarán storm) (Fig. S2).

The four sampled ponds are situated in the periphery of the city of Brussels, with the Silex pond being bordered by the Sonian Forest (Fig. 1). The four ponds are relatively small (0.7-3.2 ha) and shallow (0.6-1.4 m) and have not been drained or dredged since at least 2018 (Table S2). The four studied ponds had significantly different Chl-*a* concentration values during summer, with the Leybeek pond having higher Chl-*a* (78.8±49.5 µg L^{-1}), followed by the Pêcheries pond (19.1±13.7 µg L^{-1}), the Tenreuken pond (3.3±2.4 µg L^{-1}), and the Silex pond (1.0±1.2 µg L^{-1}) (Figs. 1, 3, Table S3). The Leybeek and Pêcheries ponds with higher summer Chl-*a* concentration had turbid-water (summer TSM = 48.7±36.2 and 13.7±10.7 mg L^{-1}, respectively), and undetectable submerged macrophyte cover in summer (Fig. 1, Table S1). The Tenreuken and Silex ponds

with lower summer Chl-*a* concentrations had clear-water (summer TSM = 4.9±3.2 and 4.0±3.2 mg L^{-1}, respectively), and a high total macrophyte cover during summer (68 and 100%, respectively, Fig. 1, Table S1). Seasonally, the highest values of Chl-*a* were observed in summer in the turbid-water Leybeek and Pêcheries ponds, related to algal blooms. Conversely, lowest values of Chl-*a* were observed in summer in the clear-water Tenreuken and Silex ponds (Figs. 1, 3), probably related to competition for dissolved inorganic nutrients with macrophytes.

The $\%O_2$ values ranged from 11 to 191% (Fig. 3). The highest $\%O_2$ values in the four ponds were observed in spring and summer compared to fall and winter owing to aquatic primary production. In summer, $\%O_2$ was significantly higher in the Leybeek pond (109±46%) characterized by higher Chl-*a* concentration compared to the Pêcheries pond (75±23%, p=0.0212, Table S3). The lowest average $\%O_2$ was observed in fall in the Pêcheries pond (46±22%) and was significantly lower than in the Leybeek (85±34%, p=0.0146, Table S3) and Silex ponds (81±19%, p=0.0130, Table S3).

The pCO_2 values ranged from 40 to 13,804 ppm (Fig. 3). Undersaturation of CO_2 with respect to atmospheric equilibrium (~410 ppm) was only observed on five occasions out of the 187 measurements, three times in the turbid-water Leybeek pond in summer (40 ppm on 13 August 2021, 220 ppm on 27 June 2022 and 149 ppm on 13 June 2023), and twice in the clear-water Tenreuken pond in spring and summer (383 ppm on 13 August 2021 and 55 ppm on 2 May 2022). Low values of pCO_2 were generally observed in spring and summer and high values of pCO_2 were observed in fall in the four ponds (Fig. 3). In summer, pCO_2 was lower in the Leybeek pond (2187±2012 ppm) than in the Pêcheries (3427±1672 ppm, p=0.0015, Table S3), and the Silex (3222±1175 ppm, p=0.0002, Table S3) ponds. When data were pooled, pCO_2 was negatively influenced by $\%O_2$, and positively by DIN, SRP, and precipitation (Table S4). In individual ponds, pCO_2 was negatively influenced by $\%O_2$ and positively by precipitation in the four ponds, positively by DIN in the Leybeek pond, by DIN and SRP in the Tenreuken pond, and negatively by Chl-*a* in the Silex pond (Table S5).

The CH_4 dissolved concentrations ranged from 194 to 48,380 nmol L^{-1} (Fig. 3) and was always above saturation (~2 nmol L^{-1}). High values of CH_4 dissolved concentrations were generally observed in spring and summer and low values of CH_4 dissolved concentrations were generally observed in winter in the four ponds (Fig. 3). In summer, CH_4 dissolved concentration was higher in the Silex pond (4,898±3,384 nmol L^{-1}) than in the Pêcheries (2,518±2,105 nmol L^{-1}, p=0.0385, Table S3) and the Tenreuken (2,189±1,365 nmol L^{-1}, p=0.0055, Table S3) ponds. When data were pooled, dissolved CH_4 concentration was influenced positively by T_W (Table S4). In individual ponds, CH_4 dissolved concentration was also influenced positively by T_W in each of the four ponds (Table S5). Additionally, CH_4 dissolved concentration was positively influenced by precipitation in the Leybeek pond and by SRP in the Silex pond, and negatively by DIN in the Pêcheries pond and by Chl-*a* in the Tenreuken and the Silex ponds. (Table S5). These relationships between CH_4 and other variables (SRP, DIN, Chl-*a*) probably indirectly reflected the seasonal variations of these other variables that were also influenced by T_W. Indeed, DIN was negatively influenced T_W in the Pêcheries pond; Chl-*a* was negatively influenced by T_W in the Tenreuken and the Silex ponds; SRP was positively influenced by T_W in the Silex pond (Table S6).

The $\%N_2O$ values ranged from 32 to 826% (Fig. 3). Undersaturation of N_2O with respect to atmospheric equilibrium was observed 66 times out of the 187 measurements. Low values of $\%N_2O$ were generally observed in spring and summer and high values of $\%N_2O$ were generally observed in fall and winter in the four ponds (Fig. 3). During spring, $\%N_2O$ was lower in the Pêcheries pond (90±11%) than the Leybeek (138±30%, p=0.0043, Table S3) and the Tenreuken (138±41, p=0.0057, Table S3) ponds. During summer, $\%N_2O$ was lower in the Pêcheries pond (78±17%) than the Leybeek (191±104%, p<0.0001, Table S3) and the Silex (126±49%, p=0.001, Table S3) pond, and lower in the Tenreuken pond (133±106%) than the Leybeek pond (p=0.0219, Table S3). During fall, $\%N_2O$ was lower in the Pêcheries pond (103±33%) than the Leybeek

pond (190±70%, p=0.0174, Table S3). For the all sampling period, $\%N_2O$ was lower in the Pêcheries pond (94±28%) than the Leybeek (178±82 %, p<0.0001, Table S7), the Tenreuken (140±77%, p<0.0001, Table S7), and the Silex (144±113%, p<0.0001, Table S7) ponds, and was lower in the Tenreuken pond than the Leybeek pond (p=0.0038, Table S7). When data were pooled, $\%N_2O$ was influenced negatively by T_W and positively by DIN and NH_4^+ (Table S4). In individual ponds, $\%N_2O$ was influenced negatively by T_W in the Leybeek, the Pêcheries, and the Tenreuken ponds (Table S5). $\%N_2O$ was influenced positively by NO_3^- in the Leybeek pond and by NH_4^+ in the Pêcheries and Tenreuken ponds (Table S8). $\%N_2O$ was influenced positively by Chl-*a* and TSM in the Tenreuken pond, and negatively by Chl-*a* in the Leybeek pond (Table S5), probably reflecting the negative influence on Chl-*a* and TSM by T_W in the Tenreuken pond and the positive influence on Chl-*a* by T_W in the Leybeek pond (Table S6).

3.2. Drivers of bubble flux

The F_{bubble} measured with inverted funnels in the four sampled ponds in the city of Brussels ranged between 0 and 2078 ml m^{-2} d^{-1} and was influenced positively by T_W in all four systems (Fig. 4). The mean $\%CH_4$ of the bubbles in the four sampled ponds in the city of Brussels was 31±21%, and values were influenced positively by T_W in the Silex pond (Fig. 4). The $\%CH_4$ of the bubbles was correlated with F_{bubble} (Fig. S3) as both variables were positively influenced by T_W (Fig. 4).

The time-series at the Silex pond allowed investigating in more detail the effects of T_W and atmospheric pressure variations on F_{bubble} (Fig. 5). In spring 2022, the F_{bubble} at the Silex pond increased during drops in atmospheric pressure (depressions) (Fig. 5). There was no relation between wind speed and peaks of F_{bubble} (r^2 = 0.01, p=0.463), suggesting a more important role of changes of atmospheric pressure than of wind speed in triggering bubble fluxes in the Silex pond in spring 2022. The F_{bubble} values at the Silex pond was higher in summer (1152±433 mL m^{-2} d^{-1}) than during spring (198±170 mL m^{-2} d^{-1}) and the temporal changes of F_{bubble} tracked those of T_W (Fig. 5). In order to evaluate the relative importance of changes of atmospheric pressure and water temperature in triggering bubble fluxes, the F_{bubble} was modelled as function of T_W alone or as function of both T_W and Δp (Figs. 5, S4). For periods of low T_W (<15°C), the inclusion of the term of Δp in the model improved the performance of the model by comparison to the measurements (Figs. 5, S4). But for warmer periods (>15°C), when bubbling fluxes were quantitatively more important, the inclusion in the model of the term of Δp did not improve the performance of the model (Figs. 5, S4). For the full T_W range (<15°C and >15°C), the inclusion of the term of Δp only improved the performance of the model very marginally (Fig. S4).

3.3. Drivers of methane ebullitive fluxes

The E_{CH4} values in the four ponds ranged between 0 and 59 mmol m^{-2} d^{-1} and were positively related to T_W (Fig. 6). The fitted relations between E_{CH4} and T_W were specific to each pond and encompassed the fitted relations established in similar systems: four small ponds in Québec (DelSontro et al., 2016) and a small urban pond in the Netherlands (Aben et al., 2017). The Q_{10} of CH_4 ebullition values ranged between 4.4 in the deeper Pêcheries pond and 26.9 in the shallower Leybeek pond (Table S9). The Q_{10} of CH_4 ebullition in the four studied ponds of the city of Brussels, in Québec (DelSontro et al., 2016), and in the Netherlands (Aben et al., 2017) were negatively related to water depth (Fig. 6).

3.4. Relative contribution of methane ebullitive and diffusive fluxes

Diffusive CH_4 fluxes computed from dissolved CH_4 concentration and *k* derived from wind speed ranged between 0.1 and 19.7 mmol m^{-2} d^{-1} (Fig. 7). The diffusive CH_4 fluxes tended to be higher in summer and spring than in fall and winter owing to the strong positive influence on CH_4 dissolved concentration by T_W (Fig. 3; Tables S4, S5). In addition, wind speed only showed small seasonal variations during sampling (0.6±0.6m s^{-1} in spring, 0.3±0.2 m s^{-1} in summer, 0.7±0.7 m s^{-1} in fall, and

0.6±0.2 m s^{-1} in winter) (Fig. S2). E_{CH4} values were calculated from the relations with T_W for each pond given in Figure 6 from the T_W data coincident with the diffusive CH_4 fluxes (Fig. 7). The resulting calculated E_{CH4} values allowed to compare and integrate seasonally both components of CH_4 emissions to the atmosphere, and to calculate the relative contribution of E_{CH4} to total (diffusive+ebullitive) CH_4 emissions. The relative contribution of E_{CH4} to total CH_4 emissions ranged between 1 and 99% in the four sampled ponds in the city of Brussels (Fig. 7) and was influenced positively by T_W (Fig. S5). The values of Q_{10} of diffusive CH_4 fluxes were lower than those for E_{CH4} in each pond, and less variable seasonally (1.2 in the Pêcheries pond to 2.9 in the Silex pond) (Table S9).

The annually averaged diffusive and ebullitive fluxes of CH_4 in the four ponds in the city of Brussels were plotted against annually averaged Chl-*a* concentration, total macrophyte cover in summer, water depth, and lake surface area (Fig. 8) that are frequent predictors of variations of CH_4 fluxes among lakes and ponds (Holgerson and Raymond, 2016; DelSontro et al., 2018, Deemer and Holgerson, 2021; Casas-Ruiz et al., 2021; Borges et al., 2022). The annually averaged E_{CH4} values were significantly higher in the two clear-water ponds (7.3±2.9 and 13.4±3.7 mmol m^{-2} d^{-1} in the Tenreuken and the Silex ponds, respectively) than the two turbid-water ponds (3.8±3.2 and 2.5±1.4 mmol m^{-2} d^{-1} in the Leybeek and the Pêcheries ponds, respectively) (Table S7). The annually averaged E_{CH4} values were significantly higher in the Silex pond, that showed a higher macrophyte cover during summer (100% in the Silex pond and 68% in the Tenreuken pond), than the Tenreuken pond ($p<0.0001$, Table S7) and were not significantly different in the two turbid-water Leybeek and Pêcheries ponds ($p=0.0617$, Table S7) that showed similar low macrophyte cover during summer (6 and 9% in the Leybeek and Pêcheries ponds, respectively) (Fig. 8). The annually averaged E_{CH4} values were overall influenced positively by macrophyte cover and negatively by Chl-*a* (Fig. 8).

In the four sampled urban ponds, annually averaged CH_4 diffusive fluxes were higher in the pond with the highest total macrophyte cover in the clear-water ponds, and higher in the pond with the highest Chl-*a* concentration in the turbid-water ponds (Fig. 8). The annually averaged relative contribution of E_{CH4} to total CH_4 emissions were higher in the two clear-water ponds than the two turbid-water ponds (Table S7). The relative contribution of E_{CH4} to the total CH_4 flux was influenced positively by macrophyte cover and negatively by Chl-*a* (Fig. 8).

The annually averaged diffusive fluxes of CO_2 (F_{CO2}) and N_2O (F_{N2O}) in the four ponds in the city of Brussels were also plotted against annually averaged Chl-*a* concentration, total macrophyte cover in summer, water depth, and lake surface area (Fig. S6). Annually averaged F_{CO2} were lower in the Leybeek pond than the Pêcheries and the Silex ponds (Table S7). F_{CO2} was not significantly influenced by the other variables (Chl-*a* concentration, total macrophyte cover, water depth, and lake surface area) (Fig. S6). Annually averaged F_{N2O} was not significantly different between clear-water and turbid-water ponds. F_{N2O} was significantly lower in the deeper Pêcheries pond than the two shallower Leybeek and Silex ponds (Table S7), and F_{N2O} showed a significant negative relationship with water depth (Fig. S6).

3.5. Relative contribution of CO_2, CH_4 and N_2O emissions

The emissions in CO_2-eq for the 3 GHGs averaged per season for both 2022 and 2023 peaked seasonally in summer in the Silex (2.9 mg CO_2-eq m^{-2} d^{-1}), the Tenreuken (1.7 mg CO_2-eq m^{-2} d^{-1}), and the Leybeek (1.1 mg CO_2-eq m^{-2} d^{-1}) pond (Fig. 9), but peaked in fall in the Pêcheries pond (1.3 mg CO_2-eq m^{-2} d^{-1}). The higher value of the total GHG emissions in fall compared to other seasons in the Pêcheries pond was due to an increase of CO_2 emissions in fall that surpassed the peak of CH_4 emissions in summer. The GHG fluxes were lowest in winter in the Silex (1.3 9 mg CO_2-eq m^{-2} d^{-1}), the Tenreuken (0.9 mg CO_2-eq m^{-2} d^{-1}), the Pêcheries (0.8 mg CO_2-eq m^{-2} d^{-1}), and the Leybeek (0.6 mg CO_2-eq m^{-2} d^{-1}) ponds. The relative

contribution of E_{CH4} peaked in summer in the Silex (73.8%), the Tenreuken (70.9%), the Pêcheries (23.6%), and the Leybeek (58.3%) ponds. The relative contribution of E_{CH4} was lowest in winter in the Silex (22.1%), the Tenreuken (10.0%), the Pêcheries (6.7%), and the Leybeek (1.0%) ponds.

The annual emissions in CO_2-eq of the three GHGs (CO_2, CH_4, and N_2O) in 2022 and 2023 were higher in the two clear-water ponds (1.3±0.5 and 1.8±0.9 mg CO_2-eq m^{-2} d^{-1} in the Tenreuken and Silex ponds, respectively) than in the two turbid-water ponds (1.0±0.2 and 0.9±0.5 mg CO_2-eq m^{-2} d^{-1} in the Leybeek and Pêcheries ponds, respectively) (Fig. 9) due to higher total CH_4 emissions (diffusive+ebullitive) in clear-water ponds (0.7±0.4 and 1.2±0.5 mg CO_2-eq m^{-2} d^{-1} in the Tenreuken and Silex ponds, respectively) than in turbid-water ponds (0.2±0.2 and 0.4±0.3 mg CO_2-eq m^{-2} d^{-1} in the Leybeek and Pêcheries ponds, respectively). The contribution of N_2O to the total GHG emissions was marginal and did not affect the differences in total GHG fluxes between ponds, with the highest contribution observed in the Leybeek pond, with a contribution of 1.7%.

The majority of GHG emissions in CO_2-eq was related to CO_2 and CH_4 (diffusive+ebullitive) in the four ponds. In turbid-water ponds CO_2 represented the largest fraction of GHG emissions (68.5% (2022) and 79.3% (2023) in the Pêcheries pond, and 49.0% (2022) and 58.3% (2023) in the Leybeek pond). In clear-water ponds CH_4 represented the largest fraction of GHG emissions (66.5% (2022) and 63.3% (2023) in the Silex pond, and 60.8% (2022) and 50.0% (2023) in the Tenreuken pond). The higher annual GHG emissions in CO_2-eq from the two clear-water ponds than from the turbid-water ponds were related to the higher contribution of E_{CH4}.

The annual GHG fluxes increased from 2022 to 2023 due to an increase in the relative contribution of CO_2 diffusive emissions in all four ponds. Diffusive CO_2 emissions averaged annually in all four ponds 0.5 mg CO_2 m^{-2} d^{-1} in 2022 and 0.7 mg CO_2 m^{-2} d^{-1} in 2023. Diffusive CO_2 emissions were 2.1 times higher in summer 2023 than in summer 2022, and 2.5 times higher in fall 2023 than in fall 2022, and showed similar values between 2023 and 2022 in spring and winter (1.1 higher and 1.1 lower, respectively).

4. Discussion

The Leybeek and Pêcheries ponds are turbid-water systems (high Chl-*a* and TSM values, low submerged macrophyte cover) and the Tenreuken and Silex ponds are clear-water systems (low Chl-*a* and TSM values, high submerged macrophyte cover) (Figs. 1, 3). All four ponds have a relatively similar size (0.7 to 3.2 ha) and depth (0.5 to 1.4 m) and are uniformly located in an urban landscape in the city of Brussels. It can be assumed that, among the four systems, the major difference that is expected to affect GHG emissions is the dominance of aquatic primary producer, either phytoplankton or macrophytes, corresponding to two alternative states *sensu* Scheffer et al. (1993). Our data-set provides the opportunity to investigate the effect of the two alternative states on GHG emissions from small lentic systems.

The reported pCO_2 values (40 to 13,804 ppm) (Fig. 3) in the four ponds in the city of Brussels were within the range of values typically observed in ponds (Holgerson and Raymond, 2016; Peacock et al., 2019; Audet et al., 2020) (Fig. 3). The pCO_2 values were influenced negatively by $\%O_2$ and positively by DIN and SRP across seasons (Tables S4, S5) showing that their seasonal variability was driven by aquatic primary production and degradation of organic matter (*e.g.* Holgerson 2015). Accordingly, low values of pCO_2 were generally observed in spring and summer probably due to uptake of CO_2 by primary production from either phytoplankton or submerged macrophytes. High values of pCO_2 were observed in fall in the four ponds and probably reflect the release of CO_2 from degradation of organic matter due to the senescence of phytoplankton or macrophytes (Fig. 3). In all four ponds, pCO_2 values were influenced positively by precipitation (Tables

S4, S5) suggesting an additional control of external inputs of carbon either as organic carbon sustaining internal degradation of organic matter or as soil CO_2 (*e.g.* Marotta et al., 2010; Ojala et al., 2011; Rasilo et al., 2012; Vachon and del Giorgio, 2014; Holgerson, 2015). The $\%N_2O$ values (32 to 826%) (Fig. 3) in the four ponds were within the range of values typically observed in ponds (Audet et al., 2020; Rabaey and Cotner, 2022). When all the data were pooled, the $\%N_2O$ was influenced positively by DIN (Table S4) as also frequently reported by other studies in ponds and interpreted as a control of nitrification and/or denitrification (hence N_2O production) by DIN levels (Audet et al., 2020; Webb et al., 2021; Wang et al., 2021; Xie et al., 2024). The negative influence on $\%N_2O$ by T_W (Table S4) might reflect the effect of the inhibition at low temperatures of the final step of denitrification leading to an accumulation of N_2O (Velthuis and Veraart, 2022) but could also indirectly result from the higher DIN concentrations observed at low T_W values (Table S6). The CH_4 dissolved concentrations (194 to 48,380 nmol L^{-1}) (Fig. 3) in the four ponds were within the range of values typically observed in ponds (Natchimuthu et al., 2014; Holgerson and Raymond, 2016; Peacock et al., 2019; Audet et al., 2020; Rabaey and Cotner, 2022; Ray et al., 2023), and were influenced positively by T_W in all four ponds individually and when pooled (Tables S4, S5), most probably reflecting the increase of sedimentary methanogenesis with temperature (Schulz and Conrad, 1996).

Temperature also exerted a strong control on bubble flux from sediments and ebullitive CH_4 emissions. The F_{bubble} values (0 and 2078 ml m^{-2} d^{-1}) in the four sampled ponds (Fig. 4) were within the range of values reported in lentic systems of equivalent size by Wik et al. (2013) (0 to 2772 mL m^{-2} d^{-1}), Delsontro et al. (2016) (11 to 748 mL m^{-2} d^{-1}), and Ray and Holgerson (2023) (0 to 2079 mL m^{-2} d^{-1}). The F_{bubble} was influenced positively by T_W (Fig. 4) in agreement with previous studies (*e.g.* Wik et al., 2013; DelSontro et al., 2016; Aben et al., 2017; Ray and Holgerson, 2023). Bubbling events from lake sediments are known to also be triggered by a decrease of hydrostatic pressure on the sediments due to water level fluctuations or drops in atmospheric pressure (Tokida et al., 2007; Scandella et al., 2011; Varadharajan and Hemond, 2012; Wik et al., 2013; Taoka et al., 2020; Zhao et al., 2021). In the Silex pond, in spring 2022, some peaks in F_{bubble} were related to drops in atmospheric pressure (Fig. 5) but unrelated to wind speed as shown in Gatun Lake (Keller and Stallard, 1994). A statistical model of F_{bubble} that included the contributions of T_W and Δp was used to quantify the relative importance of each of these two drivers (Fig. S4) and showed that air pressure drop seemed quantitatively important only at low T_W and that the intensity of bubble flux was mainly driven by temperature change at yearly scales, in agreement with previous studies (*e.g.* Wik et al., 2013; DelSontro et al., 2016; Aben et al., 2017; Ray and Holgerson, 2023).

The mean $\%CH_4$ of the bubbles (31±21%) in the four sampled ponds in the city of Brussels was comparable to the values obtained by Wik et al. (2013) (35±25%), Delsontro et al. (2016) (58±25%), and Ray and Holgerson (2023) (25±13%) in lentic systems of similar size. The increasing pattern of $\%CH_4$ of the bubbles with T_W (Fig. 4) was most probably related to the strong dependence of methanogenesis on temperature (Schulz and Conrad, 1996). The increase of methanogenesis with temperature leads to the build-up of gas bubbles in sediments that are richer in CH_4, and consequently to higher bubble fluxes with a higher CH_4 content at higher temperatures (Figs. 4, S3). Since both F_{bubble} and the $\%CH_4$ of the bubbles increased with T_W (Fig. 4), E_{CH4} in the four ponds were also positively related to T_W (Fig. 6) as shown previously in other small lentic systems (*e.g.* Wik et al., 2013; DelSontro et al., 2016; Natchimuthu et al., 2016; Aben et al., 2017; Ray and Holgerson, 2023; Rabaey and Cotner, 2024). Yet, the dependency of CH_4 ebullition on temperature (Q_{10}) was different among the four ponds and was negatively related to depth including data from systems in Québec (DelSontro et al., 2016) and The Netherlands (Aben et al., 2017) (Fig. 6). This implies that an increase in T_W leads to a smaller increase in CH_4 ebullitive fluxes (lower Q_{10}) in deeper ponds as the impact of hydrostatic pressure on sediments is higher in deeper ponds compared to shallow ponds, restricting bubble formation and release (*e.g.* DelSontro et al., 2016). This dependence of Q_{10} of

CH_4 ebullition to depth suggests that the response of CH_4 ebullition to heatwaves (or longer-term warming) might be more intense the shallower the pond, in addition to other effects from heat-waves on GHG emissions (*e.g.* Audet et al., 2017).

The values of Q_{10} for diffusive CH_4 fluxes in the four ponds were lower than those for ebullitive CH_4 fluxes (Table S9) as reported by other studies in lentic systems (DelSontro et al., 2016; Xun et al., 2024). The lower dependence to T_W of diffusive CH_4 fluxes compared to ebullitive CH_4 fluxes might be related to a lower relative change of CH_4 concentrations and k with the variation of T_W. Dissolved CH_4 concentrations in surface waters of lentic systems are strongly affected by microbial methane oxidation (*e.g.* Bastviken et al., 2002). A relative increase of methanogenesis in sediments might lead to a stronger increase of CH_4 emission by ebullition than by diffusion because of a reduction of CH_4 diffusive emissions resulting from microbial methane oxidation. Additionally, k depends on wind speed, but in the four ponds, the warmer periods of the year (summer) tended to be less windy (~0.3 m s^{-1}) than the other seasons (>0.6 m s^{-1}) also contributing to a lower dependence on T_W of CH_4 diffusive fluxes compared to ebullitive fluxes (lower Q_{10} values).

The difference in the Q_{10} of diffusive and ebullitive CH_4 fluxes was consistent with a variable contribution of the diffusive and ebullitive CH_4 fluxes seasonally as a function of T_W. The contribution of E_{CH4} to total (diffusive+ebullitive) CH_4 emissions strongly increased with T_W in the four ponds (Fig. S5). At annual scale, E_{CH4} represented between 55% and 83% of the total CH_4 emissions in the Leybeek and Silex ponds, respectively. This finding is consistent with other studies showing that ebullitive CH_4 fluxes can account for more than half of total CH_4 emissions in small and shallow lentic systems (*e.g.* Wik et al., 2013; Deemer and Holgerson, 2021; Ray and Holgerson, 2023; Rabaey and Cotner, 2024). The averaged E_{CH4} values were higher in the two clear-water ponds (10.4 mmol m^{-2} d^{-1}) than the two turbid-water ponds (3.2 mmol m^{-2} d^{-1}) (Fig 7). The averaged E_{CH4} values in the four ponds were influenced positively by macrophyte cover and negatively by Chl-*a* (Fig. 8). The higher E_{CH4} values from the two clear-water ponds would suggest that the delivery of organic matter to sediments from macrophytes sustained a quantitatively larger methane production than from phytoplankton. This finding is consistent with the notion that vegetated littoral zones of lakes are hot spots of CH_4 production and emission (*e.g.* Hyvönen et al., 1998; Huttunen et al., 2003; Juutinen et al., 2003; Desrosiers et al., 2022). CH_4 fluxes in lentic systems have been extrapolated at global scale assuming a dependency on aquatic productivity using Chl-*a* as a predictor (*e.g.* DelSontro et al., 2018). The negative relation between E_{CH4} values with Chl-*a* (Fig. 8) shows that Chl-*a* concentration alone fails to predict ebullitive fluxes in macrophyte-dominated clear-water ponds.

The annually averaged diffusive CH_4 emissions in the four ponds seemed to respond positively to both increasing phytoplankton and macrophyte biomass resulting in a U-shaped relation between diffusive CH_4 emissions and Chl-*a* as well as macrophyte cover (Fig. 8). Higher values of annually averaged CH_4 diffusive fluxes occurred at the extreme values of Chl-*a* or of macrophyte cover (minimum or maximum), and lower values occurred at the intermediate values of Chl-*a* or macrophyte cover. Such U-shape relation resulted from the inverse relationship between macrophyte cover and Chl-*a* (alternative states) and is consistent with reported positive relation between diffusive CH_4 fluxes with both macrophyte cover (*e.g.* Ray et al., 2023; Theus et al., 2023) as well as with phytoplankton biomass (*e.g.* DelSontro et al., 2018; Yan et al., 2019; Bartosiewicz et al., 2021). The relative contribution of E_{CH4} to the total annual CH_4 flux increased with the macrophyte cover (Fig. 8), in agreement with the idea of an increase of CH_4 ebullition relative to diffusive CH_4 emissions in vegetated sediments compared to unvegetated sediments (*e.g.* Desrosiers et al., 2022; Ray et al., 2023; Theus et al., 2023).

Fluxes of CH_4 and CO_2 have been reported to be negatively related to surface area and depth by numerous studies in ponds (*e.g.* Holgerson, 2015; Holgerson and Raymond, 2016; Ray et al., 2023; Theus et al., 2023) and lakes (*e.g.* Kankaala et al., 2013; DelSontro et al., 2018, Deemer and Holgerson, 2021; Casas-Ruiz et al., 2021; Borges et al., 2022). Annual diffusive

F_{CH4} and F_{CO2} were both unrelated to surface area and depth in the four studied ponds (Figs. 8, S6) resulting from the narrow range of variation of water depth (0.6 to 1.4 m) and surface area (0.7 to 3.2 ha). The lack of relationship between annual F_{CO2} and both Chl-*a* and macrophyte cover in the four ponds (Fig. S6) might be surprising since other studies have reported lower CO_2 fluxes in more productive lentic systems (*e.g.* Sand-Jensen and Staehr, 2007; Borges et al., 2022). We hypothesize that given that the four systems were either phytoplankton-dominated or macrophyte-dominated (alternative states), the ponds had an important submerged productivity, in both cases, resulting in a relatively invariant F_{CO2} as function of either Chl-*a* or macrophyte cover.

Global average emissions of GHGs in CO_2-eq from inland waters are dominated by CO_2 followed by CH_4 with a small contribution from N_2O according to Lauerwald et al. (2023). However, in small lentic systems such as ponds, the CO_2-eq emissions from CH_4 can match or dominate those of CO_2 (*e.g.* Webb et al., 2023; Ray and Holgerson, 2023; Rabaey and Cotner, 2024). The meta-analysis of Holgerson and Raymond (2016) suggested that the CO_2 and CH_4 emissions in CO_2-eq are numerically close in small lentic systems such as ponds but become increasingly dominated by CO_2 emissions in larger lentic systems. In the four studied ponds, the GHG emissions in CO_2-eq were dominated by CO_2 and CH_4 with a marginal contribution (<2%) from N_2O (Fig. 9). Annually, CO_2 represented the largest fraction of GHG emissions in CO_2-eq (~60%) in turbid-water ponds (Leybeek and Pêcheries), while CH_4 represented the largest fraction of GHG emissions in CO_2-eq (~60%) in clear-water ponds (Silex and Tenreuken) as a result of higher E_{CH4} values in the clear-water ponds (Fig. 7).

The annual GHG emissions in CO_2-eq increased from 2022 to 2023 due to an increase in the relative contribution of CO_2 diffusive emissions in all four ponds (Fig. 9) as a result of higher precipitation in 2023 (Fig. 2). Air temperatures were similar in both years (annual average of 12.2°C in 2022 and 12.1°C in 2023), and precipitation was 1.5 times higher in 2023 than in 2022. Higher precipitation is likely to increase the inputs of organic and inorganic carbon from soils to ponds, as previously shown in other lentic systems (*e.g.* Marotta et al., 2011; Ojala et al., 2011; Rasilo et al., 2012; Vachon and del Giorgio, 2014; Holgerson, 2015). This hypothesis is only based on the comparison of two years but the increase of the relative contribution of CO_2 diffusive emissions in 2023 was observed in all four ponds. The synchronicity of the increase of CO_2 diffusive emissions in 2023 compared to 2022 suggests a common uniform driver in all four ponds that would be consistent with a large variation in weather between the two years such as annual precipitation. The strong El Niño event in 2023 induced low-level cyclonic wind anomalies and higher precipitation over Western Europe, including Belgium (Chen et al., 2024).

5. Conclusions

Ebullitive CH_4 emissions in 2022-2023 were higher in the two clear-water, macrophyte-dominated ponds (Tenreuken and Silex) than in the two turbid-water, phytoplankton-dominated ponds (Pêcheries and Leybeek) of the city of Brussels, although, the diffusive CH_4 fluxes were not significantly different between the clear-water ponds and the turbid-water ponds. The annually averaged diffusive N_2O and CO_2 fluxes were not significantly different in the two clear-water ponds from those in the two turbid-water ponds. Other studies have found no difference in N_2O sedimentary production in lakes with high and low density of submerged macrophytes. We hypothesize that CO_2 fluxes were relatively invariant among the four sampled ponds because of their similar size, depth, and putatively productivity (either from phytoplankton or submerged macrophytes). The total (diffusive and ebullitive) CH_4 emissions represented 58% of total annual GHG emissions in CO_2-eq in the two clear-water ponds compared to 41% in the two turbid-water ponds. CO_2 represented nearly all the remainder of total annual GHG emissions in CO_2-eq, and N_2O represented a very marginal fraction (<2%).

549 The seasonal variations of GHG emissions were mainly driven by CH_4 ebullitive emissions that peaked in summer (both
550 quantitatively and relatively), as CH_4 ebullition was related positively to T_W resulting from an increase in both flux of
551 bubbles and CH_4 content of bubbles with warming. The pCO_2 values in the four sampled ponds increased with precipitation
552 at seasonal scale, probably in relation to higher inputs of organic and inorganic carbon from soils. Years 2022 and 2023 were
553 abnormally dry and wet, respectively. The GHG emissions were higher in 2023 than 2022 mainly due to an increase in the
554 relative contribution of CO_2 emissions probably due to higher precipitation in response to a strong El Niño event of 2023.
555 This would suggest that variations of precipitation also affected year-to-year variations of CO_2 emissions in addition to
556 partly regulating seasonal variations of CO_2 emissions from the four studied ponds.

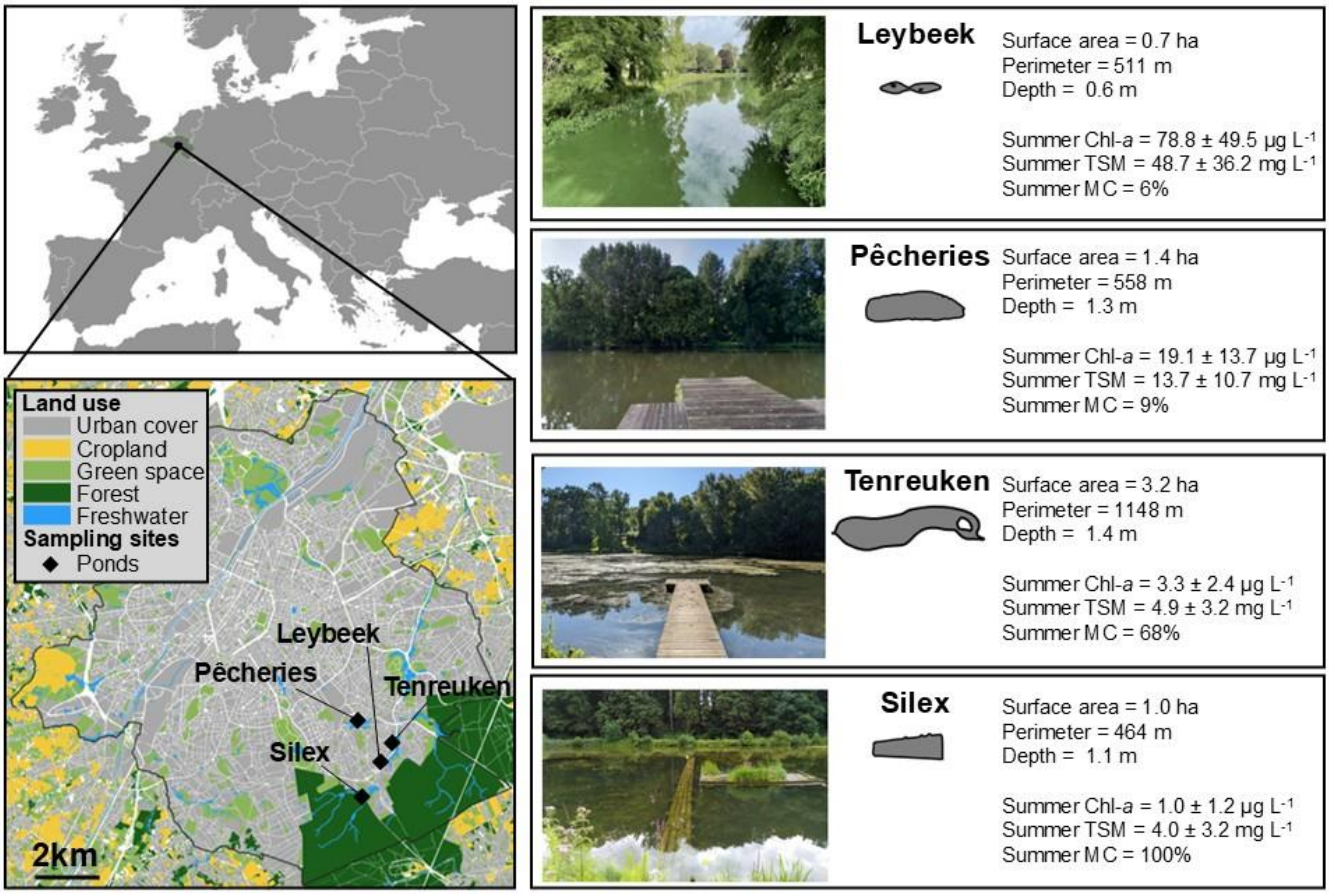

Figure 1: Location of the four sampled urban ponds (black diamonds) in city of Brussels (Belgium) delineated by the black line. Right panels indicate for each pond the shape of the ponds, surface area (ha), perimeter (m), average depth (m), mean±standard deviation of chlorophyll-*a* (Chl-*a*, in µg L^{-1}) and total suspended matter (TSM, in mg L^{-1}) in summer (21 June to 21 September in 2021, 2022, 2023), and summer total macrophyte cover (MC, in %) (Table S1).

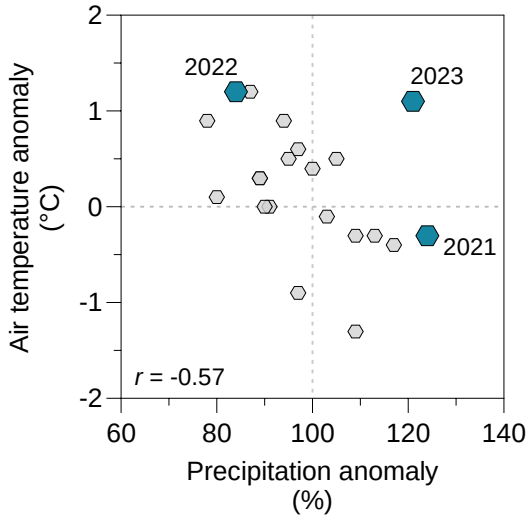

562

563 **Figure 2: Anomaly of annual air temperature (°C) as a function of anomaly of annual precipitation (%) from 2003 to 2023 with**
564 **respect to average of the 1991-2020 period (11 °C and 837 mm, respectively). Small grey hexagons represent anomaly values for**
565 **years 2003-2020 and larger blue hexagons represent anomaly values for years 2021-2023. The air temperature anomaly was**
566 **correlated to the precipitation anomaly for years 2003-2020 (Pearson *r* = -0.57, *p*=0.0147, *n*=18). Note the anomalous rainy year in**
567 **2023 relative to the pattern of precipitation as function of temperature anomalies for the other years, possibly in response to the**
568 **strong El Niño event of 2023 (Chen et al., 2024).**

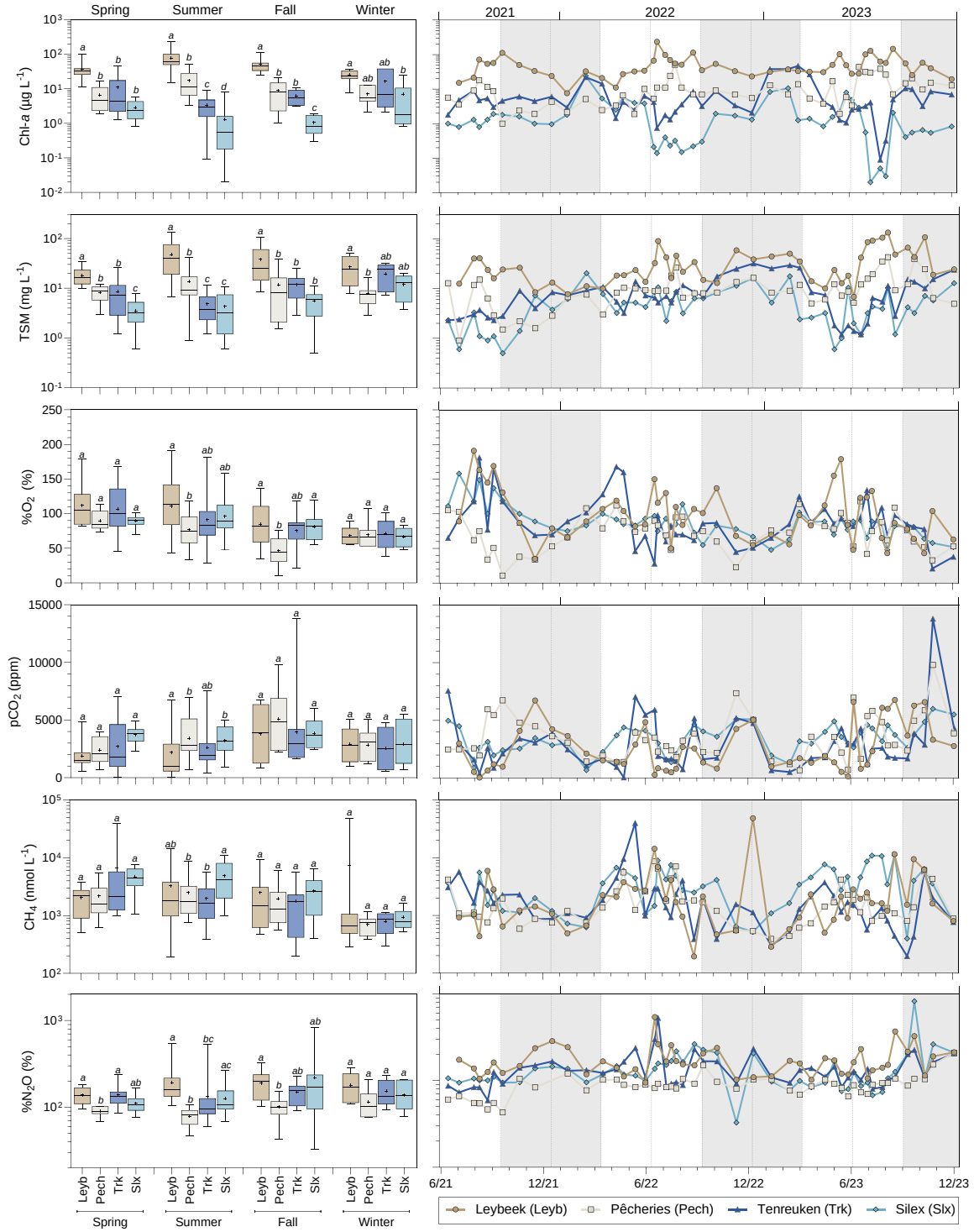

Figure 3: Seasonal variations of Chlorophyll-*a* (Chl-*a*, in µg L^{-1}), total suspended matter (TSM, in mg L^{-1}), oxygen saturation ($\%O_2$, in %), partial pressure of CO_2 (pCO_2 in ppm), dissolved CH_4 concentration (CH_4, in nmol L^{-1}), and N_2O saturation level ($\%N_2O$, in %) in four urban ponds (Leybeek (Leyb), Pêcheries (Pech), Tenreuken (Trk), and Silex (Slx)) in the city of Brussels (Belgium) from June 2021 to December 2023. Box plots show median (horizontal line), mean (cross), and 25–75% percentiles (box limits). Whiskers extend from minimum to maximum values. Grey and white bands in the plots on the right correspond to the autumn/winter and spring/summer periods, respectively, and dotted vertical bars indicate the first day of each season. Lower case letters indicate significant differences between ponds (Tables S3 and S4).

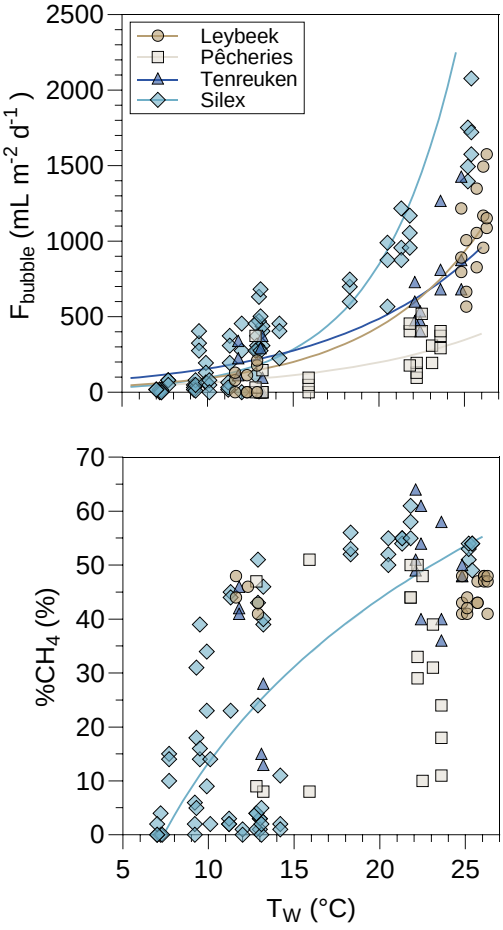

577

578 **Figure 4: Bubble flux (F_{bubble} in ml m^{-2} d^{-1}) and the relative CH_4 content in bubbles (%CH_4, in %) as a function of surface water**
579 **temperature (T_w in °C) in four urban ponds (Leybeek, Pêcheries, Tenreuken, and Silex) in the city of Brussels (Belgium) from**
580 **June 2021 to December 2023. Bubbles fluxes were measured with three bubble traps in spring, summer, and fall of 2022 and 2023,**
581 **totalling 8 days in the Leybeek, Pêcheries, and Tenreuken ponds and 24 days in the Silex pond. Given the shallowness of the**
582 **sampled systems (<1.5 m, Fig. 1), we assumed that sediments experience the same temperature as surface waters. In the upper**
583 **plot, solid lines represent linear regression of $\log_{10}(F_{bubble})$ as a function of T_W for the Leybeek ($\log_{10}(F_{bubble}) = 0.0664 \times T_W +$**
584 **1.3095, n=22, p<0.0001), the Pêcheries ($\log_{10}(F_{bubble}) = 0.0486 \times T_W + 1.3257$, n=22, p=0.0146), the Tenreuken ($\log_{10}(F_{bubble}) = 0.0492$**
585 **$\times T_W + 1.7039$, n=19, p<0.0001), and the Silex ($\log_{10}(F_{bubble}) = 0.0945 \times T_W + 1.0373$, n=72, p<0.0001) ponds. In the lower plot, solid**
586 **line represents the linear regression of %CH_4 as a function of $\log_{10}(T_W)$ for the Silex pond (%CH_4=101.11 × $\log_{10}(T_W)$ - 87.8, n=72,**
587 **p<0.0001).**

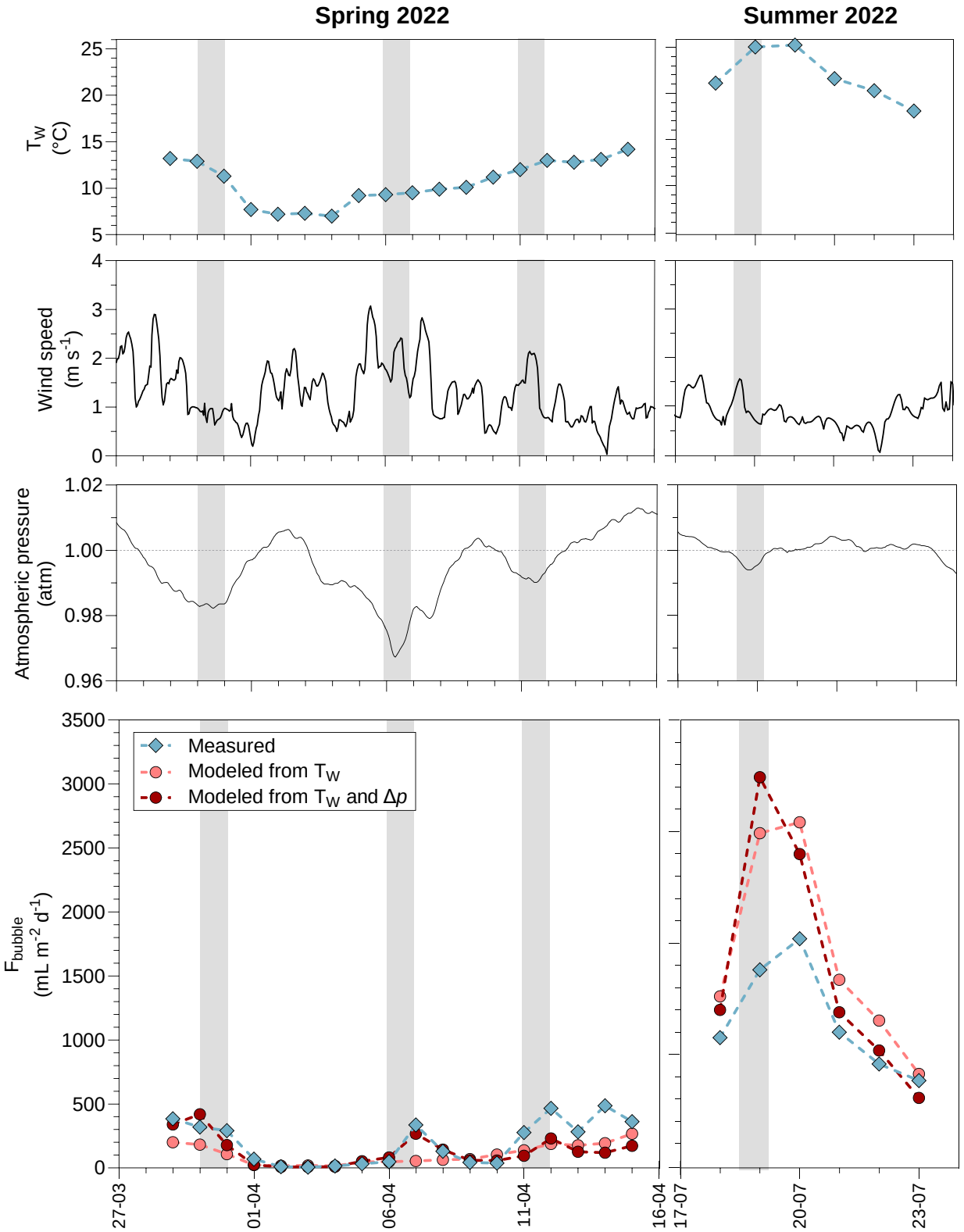

Figure 5: Time-series of surface water temperature (T_W, °C), wind speed (m s^{-1}), atmospheric pressure (atm), measured and modeled bubble flux (F_{bubble} in ml m^{-2} d^{-1}) in the Silex pond from the 29 March 2022 to the 15 April 2022 and from the 18 July 2022 to the 23 July 2022. The bubble flux was modelled from a fit to data based on Tw alone ($\log_{10}(F_{bubble}) = 3.973 \times \log_{10}(T_w) - 2.15$, p<0.0001, n=72) and based on both T_W and drops in atmospheric pressure (Δp) ($\log_{10}(F_{bubble}) = 4.551 \times \log_{10}(T_w) + 1.962 \times \Delta p - 3.006$, $p < 0.0001$, n = 72).

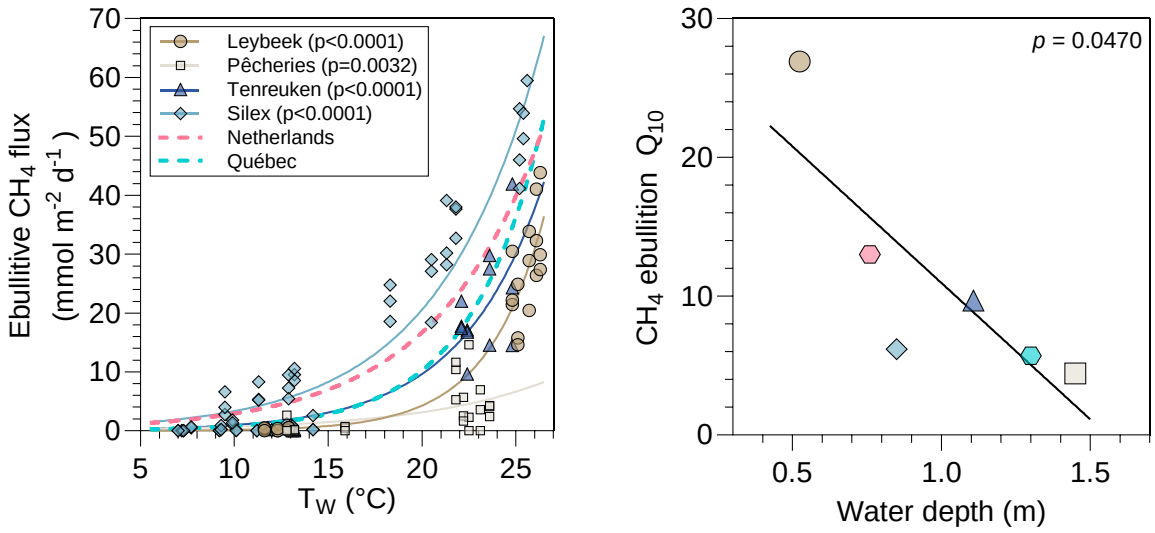

594

595 **Figure 6: Measured ebullitive CH_4 fluxes (mmol m^{-2} d^{-1}) as function of surface water temperature (°C) in four urban ponds**
596 **(Leybeek, Pêcheries, Tenreuken, and Silex) in the city of Brussels (Belgium), in spring, summer, and fall of 2022 and 2023,**
597 **totalling 8 days in the Leybeek, Pêcheries, and Tenreuken ponds and 24 days in the Silex pond, with three bubble traps. Solid lines**
598 **represent exponential fit for the Leybeek ($Y = 0.01 \cdot e^{0.32 \cdot X}$, n=22), Pêcheries ($Y = 0.16 \cdot e^{0.15 \cdot X}$, n=22), Tenreuken ($Y =$**
599 **$0.10 \cdot e^{0.23 \cdot X}$, n=19), Silex ($Y = 0.54 \cdot e^{0.18 \cdot X}$, n=72) ponds (Table S7). Dashed lines represent published exponential fit**
600 **established in similar systems: four small ponds in Québec ($Y = 0.06 \cdot e^{0.25 \cdot X}$) (DelSontro et al., 2016) and a small urban pond in**
601 **the Netherlands ($Y = 0.51 \cdot e^{0.17 \cdot X}$) (Aben et al., 2017). Each exponential curve allows to determine a Q_{10} of CH_4 ebullition,**
602 **plotted against water depth; solid line represents linear regression ($Y = 30.64 - 19.67 \cdot X, n = 6$).**

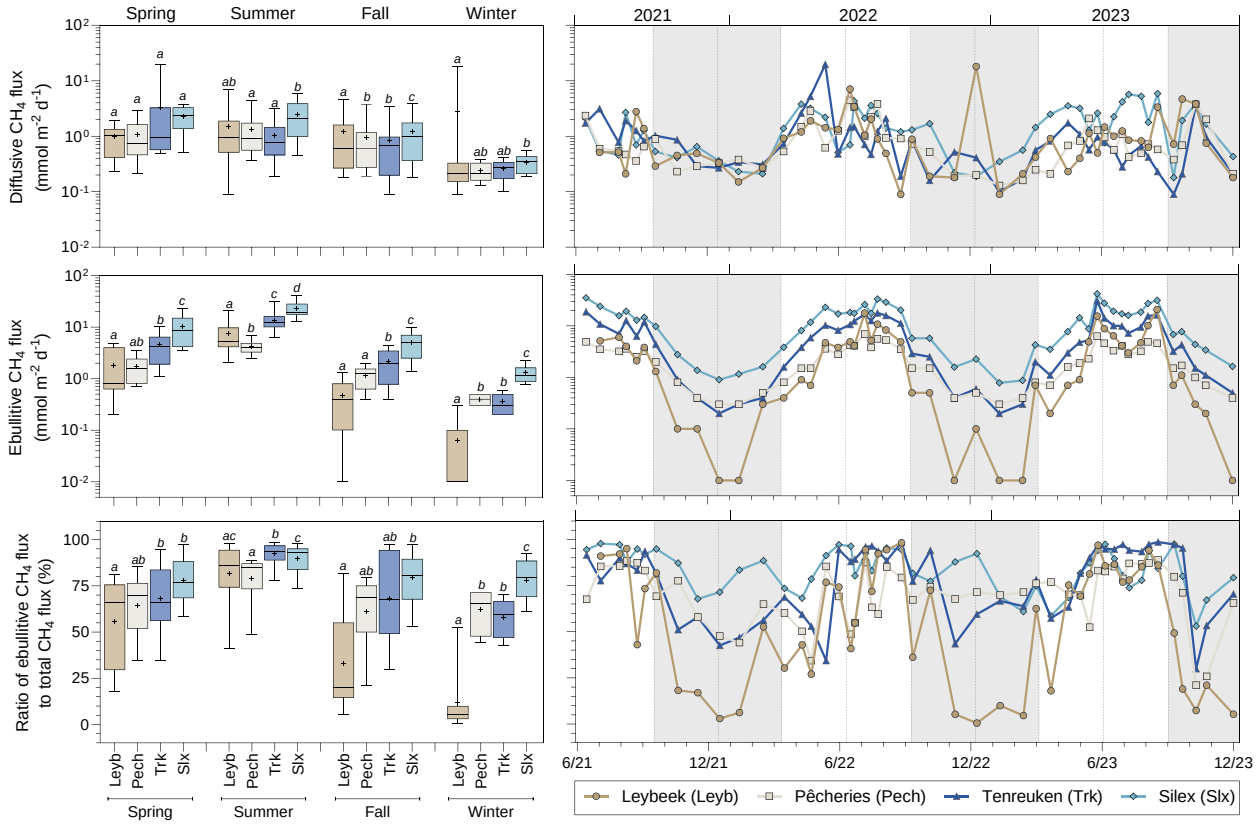

603

604 **Figure 7: Seasonal variations of diffusive and ebullitive CH_4 fluxes (mmol m^{-2} d^{-1}), and the ratio of ebullitive CH_4 flux to total**
605 **(ebullitve+diffusive) CH_4 flux (%) in four urban ponds (Leybeek (Leyb), Pêcheries (Pech), Tenreuken (Trk), and Silex (Slx)) in the**
606 **city of Brussels (Belgium) from June 2021 to December 2023. Diffusive fluxes were calculated from CH_4 concentration and gas**
607 **transfer velocity derived from wind speed. Ebullitive CH_4 fluxes were calculated from the relations with water temperature for**
608 **each pond (Fig. 6; Table S7) from the water temperature data coincident with the diffusive CH_4 fluxes. Note that the relations of**
609 **ebullitive CH_4 fluxes as a function of water temperature were established over a temperature range (7.0 to 26.3°C) that is**
610 **consistent with the range of water temperature values (2.0-25.9°C) over which the ebullitive CH_4 fluxes were modelled. Box plots**
611 **show median (horizontal line), mean (cross), and 25–75% percentiles (box limits). Whiskers extend from minimum to maximum**
612 **values. Grey and white bands in the plots on the right correspond to the autumn/winter and spring/summer periods, respectively,**
613 **and dotted vertical bars indicate the first day of each season. Lower case letters indicate significant differences between ponds**
614 **(Tables S3 and S4).**

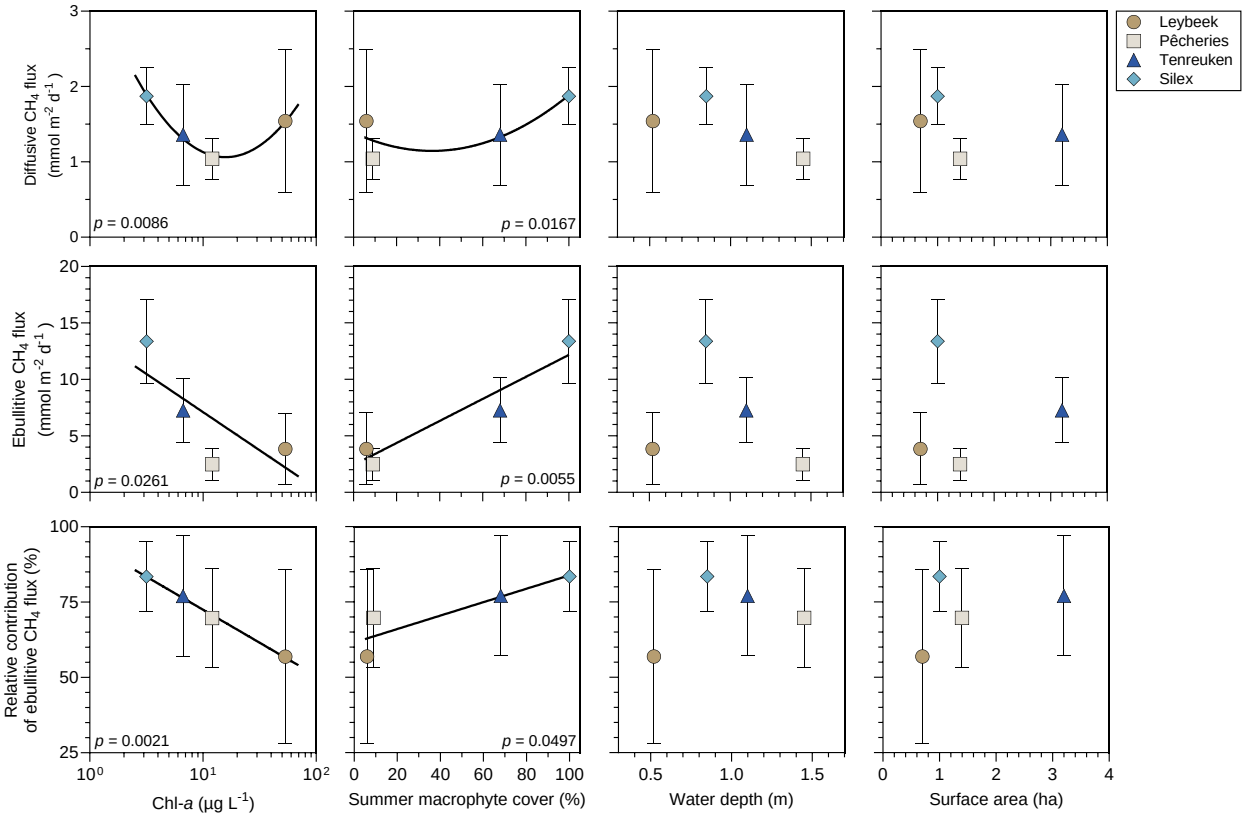

615

616 **Figure 8: Mean diffusive and ebullitive CH_4 fluxes (mmol m^{-2} d^{-1}) and mean ratio of ebullitive CH_4 flux to total**
617 **(diffusive+ebullitive) CH_4 flux (%) versus chlorophyll-*a* (Chl-*a*, in µg L^{-1}), total macrophyte cover in summer (%), water depth**
618 **(m), and lake surface area (ha) in four ponds (Leybeek, Pêcheries, Tenreuken, and Silex) in the city of Brussels (Belgium) from**
619 **June 2021 to December 2023. Error bars indicate the standard deviation. Solid lines indicate either linear or polynomial fits.**
620 **Statistical comparisons between the four ponds are summarized in Table S3.**

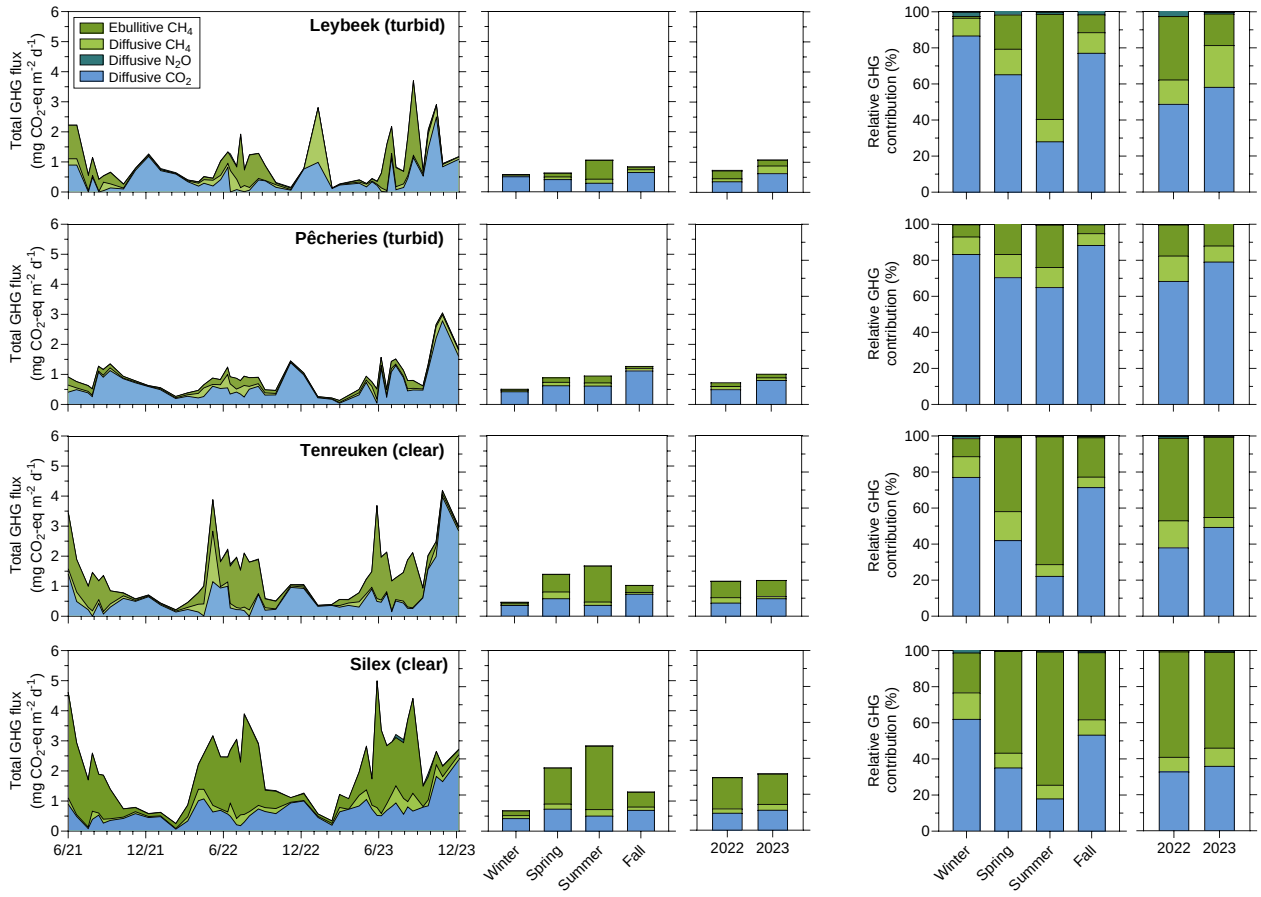

Figure 9: Seasonal and year-to-year variations of the emissions to the atmosphere of CO_2 (diffusive), CH_4 (diffusive and ebullitive), and N_2O (diffusive) expressed in CO_2 equivalents (in mg CO_2-eq m^{-2} d^{-1}) and their relative contribution in %, in four urban ponds (Leybeek, Pêcheries, Tenreuken, and Silex) in the city of Brussels (Belgium) from June 2021 to December 2023. Seasonal averages include data from 2021, 2022, and 2023. The annual precipitation was higher in 2023 (1011 mm) than in 2022 (701 mm).

Data availability. The full data-set is available at 10.5281/zenodo.11103556.

Author contributions. AVB and NG conceived the study; TB collected field samples; TB and AVB made the laboratory analysis; TB and AVB jointly interpreted data and drafted the manuscript with substantial inputs from NG.

Competing interests. The authors declare that they have no conflict of interest.

Acknowledgements. We thank Ozan Efe (University of Liège) and Adriana Anzil (Université Libre de Bruxelles) for analytical assistance, Florence Charlier (Université Libre de Bruxelles) for help in macrophyte identification and density quantification (Table S1), Bruxelles Environnement for providing information on history of operations in the ponds (Table S2), two anonymous reviewers and Associate Editor (Gabriel Singer) for comments and suggestions on the previous versions of the manuscript.

Financial support. TB received funding from the Brussels-Capital Region's institute for the encouragement of scientific research and innovation (Innoviris) as part of the Smartwater project (RBC/2020-EPF-6 h) and from the "Fonds pour la formation à la Recherche dans l'Industrie et dans l'Agriculture" (FRIA, Belgium). AVB is a Research Director at the FRS-FNRS.

References

Aben, R. C. H., Barros, N., Van Donk, E., Frenken, T., Hilt, S., Kazanjian, G., Lamers, L. P. M., Peeters, E. T. H. M., Roelofs, J.G.M., de Senerpont Domis, L. S., Stephan, S., Velthuis, M., Van de Waal, D., Wik, M., Thornton, B., Wilkinson, J., Delsontro, T., and Kosten, S.: Cross continental increase in methane ebullition under climate change. *Nature communications*, 8(1), 1682. https://doi.org/10.1038/s41467-017-01535-y, 2017.

Audet, J., Neif, É.M., Cao, Y., Hoffmann, C.C., Lauridsen, T.L., Larsen, S.E., Søndergaard, M., Jeppesen, E., and Davidson, T.A.: Heat-wave effects on greenhouse gas emissions from shallow lake mesocosms. *Freshwater Biology*. 2017; 62: 1130–1142. https://doi.org/10.1111/fwb.12930, 2017.

Audet, J., Carstensen, M.V., Hoffmann, C.C., Lavaux, L., Thiemer, K., and Davidson, T.A.: Greenhouse gas emissions from urban ponds in Denmark. *Inland Waters*, 10 (3), 373–385. https://doi.org/10.1080/20442041.2020.1730680, 2020.

Baliña, S., Sanchez, M. L., Izaguirre, I., and del Giorgio, P. A.: Shallow lakes under alternative states differ in the dominant greenhouse gas emission pathways. *Limnology and Oceanography*, 68(1), 1-13. https://doi.org/10.1002/lno.12243, 2023.

Barko, J. W., Gunnison, D., and Carpenter, S. R.: Sediment interactions with submersed macrophyte growth and community dynamics. *Aquatic botany*, *41*(1-3), 41-65. https://doi.org/10.1016/0304-3770(91)90038-7, 1991.

Bartosiewicz, M., Maranger, R., Przytulska, A., and Laurion, I.: Effects of phytoplankton blooms on fluxes and emissions of greenhouse gases in a eutrophic lake. *Water Research*, *196*, 116985. https://doi.org/10.1016/j.watres.2021.116985, 2021.

Bastviken, D., Ejlertsson, J. and Tranvik, L.: Measurement of methane oxidation in lakes: A comparison of methods. *Environmental Science & Technology*, 36, 3354-3361. https://doi.org/10.1021/es010311p, 2002.

Bastviken, D., Treat, C.C., Pangala, S.R., Gauci, V., Enrich-Prast, A., Karlson, M., Gålfalk, M., Romano, M.B., and Sawakuchi, H.O.: The importance of plants for methane emission at the ecosystem scale. *Aquatic Botany*, 184, 103596. https://doi.org/10.1016/j.aquabot.2022.103596, 2023.

Bates, D., Maechler, M., Bolker, B., and Walker, S.: Fitting linear mixed-effects models using lme4. *Journal of Statistical Software*, 67, 1–48. https://doi.org/10.1126/science.1176170, 2015.

Bauduin, T., Gypens, N., and Borges, A.V.: Seasonal and spatial variations of greenhouse gas (CO2, CH4 and N2O) emissions from urban ponds in Brussels. *Water Research*, 121257. https://doi.org/10.1016/j.watres.2024.121257, 2024.

Borges, A.V., Darchambeau, F., Lambert, T., Morana, C., Allen, G.H., Tambwe, E., and Bouillon, S.: Variations in dissolved greenhouse gases (CO2, CH4, N2O) in the Congo River network overwhelmingly driven by fluvial-wetland connectivity. *Biogeosciences*, 16 (19), 3801–3834. https://doi.org/10.5194/bg-16-3801-2019, 2019.

Borges, A.V., Deirmendjian, L., Bouillon, S., Okello, W., Lambert, T., Roland, F.A.E., Razanamahandry, V.F., Voarintsoa, N.R.G., Darchambeau, F., Kimirei, I.A., Descy, J., Allen, G.H., and Morana, C.: Greenhouse gas emissions from African lakes are no longer a blind spot. *Sciences Advances*, 8 (25), eabi8716. https://doi.org/10.1126/sciadv. abi8716, 2022.

Borges, A.V., Okello, W., Bouillon, S., Deirmendjian, S., Nankabirwa, A., Nabafu, E., Lambert, T., Descy, J-P, and Morana, C.: Spatial and temporal variations of dissolved CO2, CH4 and N2O in Lakes Edward and George (East Africa). *Journal of Great Lakes Research*, 49, 229-245, https://doi.org/10.1016/j.jglr.2022.11.010, 2023.

Brans, K.I., Engelen, J.M., Souffreau, C., and De Meester, L.: Urban hot-tubs: local urbanization has profound effects on average and extreme temperatures in ponds. *Landscape and Urban Planning*, 176, 22–29. https://doi.org/10.1016/j, 2018.

Cael, B. B., Heathcote, A. J., and Seekell, D. A.: The volume and mean depth of Earth's lakes. *Geophysical Research Letters*, *44*(1), 209-218. https://doi.org/10.1002/2016GL071378, 2017.

Casas-Ruiz, J.P., Jakobsson, J., and del Giorgio, P.A.: The role of lake morphometry in modulating surface water carbon concentrations in boreal lakes. *Environmental Research Letters*, 16 (7), 074037 https://doi.org/10.1088/1748-9326/ac0be3, 2021.

Chen, B., Zhang, L., and Wang, C.: Distinct impacts of the central and eastern Atlantic Niño on the European climate. *Geophysical Research Letters*, 51(2), e2023GL107012. https://doi.org/10.1029/2023GL107012, 2024.

Choudhury, M. I., McKie, B. G., Hallin, S., and Ecke, F.: Mixtures of macrophyte growth forms promote nitrogen cycling in wetlands. *Science of the Total Environment*, *635*, 1436-1443. https://doi.org/10.1016/j.scitotenv.2018.04.193, 2018.

Clifford, C.C., and Heffernan, J.B.: Artificial aquatic ecosystems. *Water*, 10 (8), 1096. https://doi.org/10.3390/w10081096, 2018.

Codispoti, L.A., and Christensen, J.P.: Nitrification, denitrification and nitrous oxide cycling in the eastern tropical South Pacific Ocean. *Marine chemistry*, 16 (4), 277–300. https://doi.org/10.1016/0304-4203(85)90051-9, 1985.

Cole, J.J., and Caraco, N.F.: Atmospheric exchange of carbon dioxide in a low-wind oligotrophic lake measured by the addition of SF6. *Limnology and Oceanography*, 43 (4), 647–656. https://doi.org/10.4319/lo.1998.43.4.0647, 1998.

Dan, Z., Chuan, W., Qiaohong, Z., and Xingzhong, Y.: Sediments nitrogen cycling influenced by submerged macrophytes growing in winter. *Water Science and Technology*, *83*(7), 1728-1738. https://doi.org/10.2166/wst.2021.081, 2021.

Davidson, T.A., Audet, J., Svenning, J.C., Lauridsen, T.L., Søndergaard, M., Landkildehus, F., and Jeppesen, E.: Eutrophication effects on greenhouse gas fluxes from shallow-lake mesocosms override those of climate warming. *Global Change Biology*, 21 (12), 4449–4463. https://doi.org/10.1111/gcb.13062, 2015.

Deemer, B. R., and Holgerson, M. A.: Drivers of methane flux differ between lakes and reservoirs, complicating global upscaling efforts. *Journal of Geophysical Research: Biogeosciences*, *126*(4) https://doi.org/10.1029/2019JG005600 , 2021.

DelSontro, T., Beaulieu, J. J., and Downing, J. A.: Greenhouse gas emissions from lakes and impoundments: Upscaling in the face of global change. *Limnology and Oceanography Letters*, *3*(3), 64-75. https://doi.org/10.1002/lol2.10073, 2018.

DelSontro, T., Kunz, M. J., Kempter, T., Wüest, A., Wehrli, B., and Senn, D. B.: Spatial Heterogeneity of Methane Ebullition in a Large Tropical Reservoir, *Environmental Science & Technology*, 45 (23), 9866-9873, https://doi.org/10.1021/es2005545, 2011.

DelSontro, T., Boutet, L., St-Pierre, A., del Giorgio, P.A., and Prairie, Y.T.:Methane ebullition and diffusion from northern ponds and lakes regulated by the interaction between temperature and system productivity, *Limnology and Oceanography*, 61(S1), S62-S77 https://doi.org/10.1002/lno.10335, 2016.

Deng, Hg., Zhang, J., Wu, J., Yao, X., and Yang, L.-W.: Biological denitrification in a macrophytic lake: implications for macrophytes-dominated lake management in the north of China. *Environmental Sciences and Pollution Research*, 27, 42460–42471. https://doi.org/10.1007/s11356-020-10230-3 , 2020.

Desrosiers, K., DelSontro, T., and del Giorgio, P.A.: Disproportionate Contribution of Vegetated Habitats to the CH4 and CO2 Budgets of a Boreal Lake. *Ecosystems*, 1-20. https://doi.org/10.1007/s10021-021-00730-9, 2022.

Dickson, A.G.; Sabine, C.L. and Christian, J.R.: Guide to best practices for ocean CO2 measurement. Sidney, British Columbia, North Pacific Marine Science Organization, 191pp. (PICES Special Publication 3; IOCCP Report 8). https://doi.org/10.25607/OBP-1342, 2007.

Dutton, G., Elkins II, J., Hall, B., NOAA ESRL, Earth System Research Laboratory Halocarbons and Other Atmospheric Trace Gases Chromatograph for Atmospheric Trace Species (CATS) Measurements. NOAA National Centers for Environmental Information. https://doi.org/10.7289/V5X0659V. Version 1. [Database: atmospheric nitrous oxide N2O] [2024-03–27], 2023.

Goeckner, A. H., Lusk, M. G., Reisinger, A. J., Hosen, J. D., and Smoak, J. M.: Florida's urban stormwater ponds are net sources of carbon to the atmosphere despite increased carbon burial over time. *Communications earth & environment*, *3*(1), 53, https://doi.org/10.1038/s43247-022-00384-y 2022.

Gorsky, A. L., Dugan, H. A., Wilkinson, G. M., and Stanley, E. H.: Under-ice oxygen depletion and greenhouse gas supersaturation in north temperate urban ponds. *Journal of Geophysical Research: Biogeosciences*, *129*(6), https://doi.org/10.1029/2024JG008120, 2024.

Gorsky, A.L., Racanelli, G.A., Belvin, A.C., and Chambers, R.M.: Greenhouse gas flux from stormwater ponds in southeastern Virginia (USA). *Anthropocene*, 28, 100218. https://doi.org/10.1016/j.ancene.2019.100218, 2019.

Grasset, C., Abril, G., Mendonça, R., Roland, F., and Sobek, S.: The transformation of macrophyte-derived organic matter to methane relates to plant water and nutrient contents. *Limnology and Oceanography*, *64*(4), 1737-1749, https://doi.org/10.1002/lno.11148, 2019.

Grasset, C., Sobek, S., Scharnweber, K., Moras, S., Villwock, H., Andersson, S., Hiller, C., Nydahl, A.C., Chaguaceda, F., Colom, W., and Tranvik, L.J.: The CO2-equivalent balance of freshwater ecosystems is non-linearly related to productivity. *Global Change Biology*, 26 (10), 5705–5715. https://doi.org/10.1111/gcb.15284, 2020.

Grasshoff, K., and Johannsen, H.: A new sensitive and direct method for the automatic determination of ammonia in sea water. *ICES Journal of Marine Science*, 34 (3), 516–521. https://doi.org/10.1093/icesjms/34.3.516, 1972.

Grasshoff, K., Kremling, K., and Ehrhardt, M.: Methods of Seawater Analysis: Determination of Nitrite. John Wiley & Sons, 2009.

Grinham, A., Albert, S., Deering, N., Dunbabin, M., Bastviken, D., Sherman, B., Lovelock, C.E., and Evans, C.D.: The importance of small artificial water bodies as sources of methane emissions in Queensland, Australia. *Hydrology and Earth System Sciences*, 22 (10), 5281–5298. https://doi.org/10.5194/hess-22-5281-2018, 2018.

Harpenslager, S. F., Thiemer, K., Levertz, C., Misteli, B., Sebola, K. M., Schneider, S. C., Hilt, S., and Köhler, J.: Short-term effects of macrophyte removal on emission of CO_2 and CH_4 in shallow lakes. *Aquatic Botany*, *182*, 103555. https://doi.org/10.1016/j.aquabot.2022.103555, 2022.

Hassall, C., The ecology and biodiversity of urban ponds. WIREs Water, 1: 187-206. https://doi.org/10.1002/wat2.1014, 2014.

Herrero Ortega, S., Romero Gonz´alez-Quijano, C., Casper, P., Singer, G.A., and Gessner, M.O.: Methane emissions from contrasting urban freshwaters: rates, drivers, and a whole-city footprint. *Global change biology*, 25 (12), 4234–4243. https://doi.org/10.1111/gcb.14799, 2019.

Hilt, S., Brothers, S., Jeppesen, E., Veraart, A. J., and Kosten, S.: Translating regime shifts in shallow lakes into changes in ecosystem functions and services. *BioScience, 67*(10), 928-936. https://doi.org/10.1093/biosci/bix106, 2017.

Holgerson, M., and Raymond, P.: Large contribution to inland water CO2 and CH4 emissions from very small ponds. *Nature Geoscience*, 9, 222–226. https://doi.org/10.1038/ngeo2654, 2016.

Holgerson, MA.: Drivers of carbon dioxide and methane supersaturation in small, temporary ponds, *Biogeochemistry*, 124, 305–318. https://doi.org/10.1007/s10533-015-0099-y, 2015.

Huttunen, J. T., Alm, J., Liikanen, A., Juutinen, S., Larmola, T., Hammar, T., Silvola, T., and Martikainen, P. J.: Fluxes of methane, carbon dioxide and nitrous oxide in boreal lakes and potential anthropogenic effects on the aquatic greenhouse gas emissions. *Chemosphere*, *52*(3), 609-621. https://doi.org/10.1016/S0045-6535(03)00243-1, 2003.

Hyvönen, T., Ojala, A., Kankaala, P., & Martikainen, P. J.: Methane release from stands of water horsetail (Equisetum fluviatile) in a boreal lake, *Freshwater Biology*, 40, 275– 284. https://doi.org/10.1046/j.1365-2427.1998.00351.x, 1998.

Johnson, M.S., Matthews, E., Du, J., Genovese, V., and Bastviken, D.: Methane Emission from Global Lakes: New Spatiotemporal Data and Observation-Driven Modeling of Methane Dynamics Indicates Lower Emissions. *Journal of Geophysical Research: Biogeosciences*, 127(7). https://doi.org/10.1029/2022JG006793, 2022.

Juutinen, S., Alm, J., Larmola, T., Huttunen, J. T., Morero, M., Martikainen, P. J., and Silvola, J.: Major implication of the littoral zone for methane release from boreal lakes, *Global biogeochemical cycles*, 17(4), 1117, https://doi.org/10.1029/2003GB002105, 2003.

Kankaala, P., Huotari, J., Tulonen, T., and Ojala, A.: A Lake-size dependent physical forcing drives carbon dioxide and methane effluxes from lakes in a boreal landscape. *Limnology and Oceanography*, 58:1915–1930. https://doi.org/10.4319/lo.2013.58.6.1915, 2013.

Keller, M., and Stallard, R. F.: Methane emission by bubbling from Gatun Lake, Panama, *Journal of Geophysical Research: Atmospheres*, 99(D4), 8307–8319, doi:10.1029/92JD02170, 1994.

Koroleff, J.: Determination of total phosphorus by alkaline persulphate oxidation. Methods of Seawater Analysis. Verlag Chemie, Wienheim, pp. 136–138, 1983.

Kosten, S., Roland, F., Da Motta Marques, D. M., Van Nes, E. H., Mazzeo, N., Sternberg, L. D. S., Scheffer, M., and Cole, J. J. Climate-dependent CO2 emissions from lakes. *Global Biogeochemical Cycles*, *24*(2). https://doi.org/10.1029/2009GB003618, 2010.

Lan, X., K.W. Thoning, and E.J. Dlugokencky: Trends in globally-averaged CH4, N2O, and SF6 determined from NOAA Global Monitoring Laboratory measurements [data set]. Version 2024-08, https://doi.org/10.15138/P8XG-AA10, 2024.

Lauerwald, R., Regnier, P., Figueiredo, V., Enrich-Prast, A., Bastviken, D., Lehner, B., Maavara, T., and Raymond, P.: Natural Lakes Are a Minor Global Source of N2O to the Atmosphere. *Global Biogeochemical Cycles, 33(12)*, 1564–1581. https://doi.org/10.1029/2019GB006261, 2019.

Lauerwald, R., Allen, G. H., Deemer, B. R., Liu, S., Maavara, T., Raymond, P., Alcott, L., Bastviken, D., Hastie, A., Holgerson, M.A., Johnson, M. S., Lehner, B., Lin, P., Marzadri, A., Ran, L., Tian, H., Yang, X., Yao, Y., and Regnier, P.: Inland water greenhouse gas budgets for RECCAP2: 2. Regionalization and homogenization of estimates. *Global Biogeochemical Cycles*, 37, e2022GB007658. https://doi.org/10.1029/2022GB007658, 2023.

Liu, W., Jiang, X., Zhang, Q., Li, F., and Liu, G.: Has submerged vegetation loss altered sediment denitrification, N_2O production, and denitrifying microbial communities in subtropical lakes? *Global Biogeochemical Cycles*, 32, 1195–1207. https://doi.org/10.1029/2018GB005978, 2018.

Maavara, T., Lauerwald, R., Laruelle, G. G., Akbarzadeh, Z., Bouskill, N. J., Van Cappellen, P., and Regnier, P.: Nitrous oxide emissions from inland waters: Are IPCC estimates too high? *Global Change Biology*, 25(2), 473–488. https://doi.org/10.1111/gcb.145042, 2019.

Marotta, H., Duarte, C. M., Pinho, L., and Enrich-Prast, A.: Rainfall leads to increased pCO2 in Brazilian coastal lakes. *Biogeosciences*, *7*(5), 1607-1614. https://doi.org/10.5194/bg-7-1607-2010 , 2010.

Martinez-Cruz, K., Gonzalez-Valencia, R., Sepulveda-Jauregui, A., Plascencia- Hernandez, F., Belmonte-Izquierdo, Y., and Thalasso, F.: Methane emission from aquatic ecosystems of Mexico City. *Aquatic Sciences*, 79, 159–169. https://doi.org/10.1007/s00027-016-0487-y, 2017.

Mengis, M., Gächter, R., and Wehrli, B.: Sources and sinks of nitrous oxide (N2O) in deep lakes. *Biogeochemistry*, *38*, 281-301. https://doi.org/10.1023/A:1005814020322, 1997.

Myrhe, G., Shindell, D., Bréon, F.M., Collins, W., and Al, E. Anthropogenic and natural radiative forcing. Climate Change 2013 the Physical Science Basis: working Group I Contribution to the Fifth Assessment Report of the Intergovernmental Panel on Climate Change. Chapter 8 : Anthropogenic and Natural Radiative Forcing 9781107057, 659–740. https://doi.org/10.1017/CBO9781107415324.018, 2013.

Natchimuthu, S., Panneer Selvam, B., and Bastviken, D.: Influence of weather variables on methane and carbon dioxide flux from a shallow pond. *Biogeochemistry*, 119, 403–413. https://doi.org/10.1007/s10533-014-9976-z, 2014.

Natchimuthu, S., Sundgren, I., Gålfalk, M., Klemedtsson, L., Crill, P., Danielsson, Å. and Bastviken, D. (2016), Spatio-temporal variability of lake CH4 fluxes and its influence on annual whole lake emission estimates. *Limnology and Oceanography*, 61: S13-S26. https://doi.org/10.1002/lno.10222, 2016.

Ni, M., Liang, X., Hou, L., Li, W., and He, C.: Submerged macrophytes regulate diurnal nitrous oxide emissions from a shallow eutrophic lake: A case study of Lake Wuliangsuhai in the temperate arid region of China. *Science of The Total Environment*, *811*, 152451. https://doi.org/10.1016/j.scitotenv.2021.152451, 2022.

Ojala A., Bellido J.L., Tulonen T., Kankaala P., and Huotari J.: Carbon gas fluxes from a brown-water and a clear-water lake in the boreal zone during a summer with extreme rain events, *Limnology and Oceanography*, 56, https://doi.org/10.4319/lo.2011.56.1.0061, 2011.

Ollivier, Q.R., Maher, D.T., Pitfield, C., and Macreadie, P.I.: Punching above their weight: large release of greenhouse gases from small agricultural dams. *Global change biology*, 25 (2), 721–732. https://doi.org/10.1111/gcb.14477, 2019.

Peacock, M., Audet, J., Bastviken, D., Cook, S., Evans, C.D., Grinham, A., Holgerson, M. A., Högbom, L., Pickard, A.E., Zieliński, P., and Futter, M.N.: Small artificial waterbodies are widespread and persistent emitters of methane and carbon dioxide. *Global change biology*, 27 (20), 5109–5123. https://doi.org/10.1111/gcb.15762, 2021.

Peacock, M., Audet, J., Jordan, S., Smeds, J., and Wallin, M.B.: Greenhouse gas emissions from urban ponds are driven by nutrient status and hydrology. *Ecosphere*, 10 (3), e02643. https://doi.org/10.1002/ecs2.2643, 2019.

Peretyatko, A., Symoens, J. J., and Triest, L.: Impact of macrophytes on phytoplankton in eutrophic peri-urban ponds, implications for pond management and restoration. *Belgian Journal of Botany*, 83-99. https://doi.org/10.2307/20794626 , 2007.

R Core Team (2021). R: A language and environment for statistical computing. R Foundation for Statistical Computing, Vienna, Austriaa. https://www.R-project.org/, 2021.

Rabaey, J. and Cotner, J.: Pond greenhouse gas emissions controlled by duckweed coverage. *Frontiers in environmental science*, 10, 889289 https://doi.org/10.3389/fenvs2022.889289, 2022.

Rabaey, J. and Cotner, J.: The influence of mixing on seasonal carbon dioxide and methane fluxes in ponds. *Biogeochemistry*, 1-18, https://doi.org/10.1007/s10533-024-01167-7, 2024.

Rasilo, T., Ojala, A., Huotari, J. and Pumpanen, J.: Rain Induced Changes in Carbon Dioxide Concentrations in the Soil–Lake–Brook Continuum of a Boreal Forested Catchment. *Vadose Zone Journal*, 11: vzj2011.0039. https://doi.org/10.2136/vzj2011.0039, 2012.

Ray, N. E., and Holgerson, M. A.: High Intra-Seasonal Variability in Greenhouse Gas Emissions from Temperate Constructed Ponds. *Geophysical Research Letters*, *50*(18), e2023GL104235, https://doi.org/10.1029/2023GL104235, 2023.

Ray, N. E., Holgerson, M. A., Andersen, M. R., Bikše, J., Bortolotti, L. E., Futter, M., Kokorīte, I., Law, A., McDonald, C., Mesman, J.P., Peacock, M., Richardson, D.C., Arsenault, J., Bansal, S., Cawley, K., Kuhn, M., Shahabinia, A.R., and Smufer, F.: Spatial and temporal variability in summertime dissolved carbon dioxide and methane in temperate ponds and shallow lakes. *Limnology and Oceanography*, *68*(7), 1530-1545. https://doi.org/10.1002/lno.12362, 2023.

Raymond, P. A., Hartmann, J., Lauerwald, R., Sobek, S., McDonald, C., Hoover, M., Butman, D., Striegl, R., Mayorga, E., Humborg, C., Kortelainen, P., Dürr, H., Meybeck, M., Ciais, P., and Guth, P.: Global carbon dioxide emissions from inland waters. *Nature*, 503(7476), 355–359. https://doi.org/10.1038/nature12760, 2013.

Reitsema, R. E., Meire, P., and Schoelynck, J.: The future of freshwater macrophytes in a changing world: dissolved organic carbon quantity and quality and its interactions with macrophytes. *Frontiers in Plant Science*, *9*, 301954. https://doi.org/10.3389/fpls.2018.00629 , 2018.

Rocher-Ros, G., Stanley, E. H., Loken, L. C., Casson, N. J., Raymond, P. A., Liu, S., Amatulli, G., and Sponseller, R. A.: Global methane emissions from rivers and streams. *Nature*, 621:530–535. https://doi.org/10.1038/s41586-023-06344-6, 2023.

Rosentreter, J. A., Borges, A. V., Deemer, B. R., Holgerson, M. A., Liu, S., Song, C., Melack, J., Raymond, P. A., Duarte, C. M., Allen, G. H., Olefeldt, D., Poulter, B., Battin, T. I., and Eyre, B. D.: Half of global methane emissions come from highly variable aquatic ecosystem sources. *Nature Geoscience*, 14(4), 225–230. https://doi.org/10.1038/s41561-021-00715-2, 2021.

Sand-Jensen, K., & Staehr, P. A.: Scaling of pelagic metabolism to size, trophy and forest cover in small Danish lakes. *Ecosystems*, *10*, 128-142. https://doi.org/10.1007/s10021-006-9001-z, 2007.

Scandella, B. P., Varadharajan, C., Hemond, H. F., Ruppel, C., and Juanes, R.: A conduit dilation model of methane venting from lake sediments. Geophysical Research Letters, 38(6). https://doi.org/10.1029/2011GL046768, 2011.

Scheffer, M., Hosper, S. H., Meijer, M. L., Moss, B., and Jeppesen, E.: Alternative equilibria in shallow lakes. *Trends in ecology & evolution*, *8*(8), 275-279. https://doi.org/10.1016/0169-5347(93)90254-M, 1993.

Schulz, S. and Conrad, R.: Influence of temperature on pathways to methane production in the permanently cold profundal sediment of Lake Constance. *FEMS Microbiology Ecology*, 20 l-14; https://doi.org/10.1111/j.1574-6941.1996.tb00299.x, 1996.

Singh, S.N., Kulshreshtha, K., and Agnihotri, S.: Seasonal dynamics of methane emission from wetlands. *Chemosphere-Global Change Science*, 2 (1), 39–46. https://doi.org/10.1016/S1465-9972(99)00046-X, 2000.

Stanley, E. H., Casson, N. J., Christel, S. T., Crawford, J. T., Loken, L. C., and Oliver, S. K.: The ecology of methane in streams and rivers: patterns, controls, and global significance. *Ecological Monographs*, 86(2), 146–171. https://doi.org/10.1890/15-1027, 2016.

Taoka, T., Iwata, H., Hirata, R., Takahashi, Y., Miyabara, Y., and Itoh, M.: Environmental controls of diffusive and ebullitive methane emissions at a subdaily time scale in the littoral zone of a midlatitude shallow lake. *Journal of Geophysical Research: Biogeosciences*, 125, e2020JG005753. https://doi.org/10.1029/2020JG005753, 2020.

Theus, M. E., Ray, N. E., Bansal, S., and Holgerson, M. A.: Submersed macrophyte density regulates aquatic greenhouse gas emissions. *Journal of Geophysical Research: Biogeosciences*, *128*(10), https://doi.org/10.1029/2023JG007758, 2023.

Tixier, G., M Lafont, M., L Grapentine, L., Q Rochfort, Q., and J Marsalek, J.: Ecological risk assessment of urban stormwater ponds: Literature review and proposal of a new conceptual approach providing ecological quality goals and the associated bioassessment tools, *Ecological Indicators*, 11, 1497-1506, https://doi.org/10.1016/j.ecolind.2011.03.027, 2011.

Tokida, T., Miyazaki, T., Mizoguchi, M., Nagata, O., Takakai, F., Kagemoto, A., and Hatano, R.: Falling atmospheric pressure as a trigger for methane ebullition from peatland. *Global Biogeochemical Cycles*, 21(2). https://doi.org/10.1029/2006GB002790, 2007.

Vachon, D., and del Giorgio, P.A. Whole-Lake CO2 Dynamics in Response to Storm Events in Two Morphologically Different Lakes. *Ecosystems*, 17, 1338–1353 (2014). https://doi.org/10.1007/s10021-014-9799-8, 2014.

Vachon, D., Langenegger, T., Donis, D., Beaubien, S. E., and McGinnis, D. F.: Methane emission offsets carbon dioxide uptake in a small productive lake. *Limnology and Oceanography Letters*, *5*(6), 384-392, https://doi.org/10.1002/lol2.10161, 2020.

van Bergen, T.J.H.M., Barros, N., Mendonça, R., Aben, R.C.H., Althuizen, I.H.J., Huszar, V., Lamers, L.P.M., Lürling, M., Roland, F., and Kosten, S.: Seasonal and diel variation in greenhouse gas emissions from an urban pond and its major drivers. *Limnology and Oceanography*, 64 (5), 2129–2139. https://doi.org/10.1002/lno.11173, 2019.

Varadharajan, C., and Hemond, H. F.: Time-series analysis of high-resolution ebullition fluxes from a stratified, freshwater lake. *Journal of Geophysical Research: Biogeosciences*, 117(G2). https://doi.org/10.1029/2011JG001866, 2012.

Velthuis, M., and Veraart, A. J.: Temperature sensitivity of freshwater denitrification and N2O emission—A meta-analysis. *Global Biogeochemical Cycles*, *36*(6), https://doi.org/10.1029/2022GB007339, 2022.

Verpoorter, C., Kutser, T., Seekell, D. A., and Tranvik, L. J.: A global inventory of lakes based on high-resolution satellite imagery. *Geophysical Research Letters*, *41*(18), 6396-6402. https://doi.org/10.1002/2014GL060641, 2014.

Wang, G., Xia, X., Liu, S., Zhang, S., Yan, W., McDowell, W.H.: Distinctive Patterns and Controls of Nitrous Oxide Concentrations and Fluxes from Urban Inland Waters, *Environmental Science & Technology*, 55, 8422–8431, https://doi.org/10.1021/acs.est.1c00647, 2021.

Wanninkhof, R.: Relationship between gas exchange and wind speed over the ocean. *Journal of Geophysical Research: Oceans*, 97, 7373–7381. https://doi.org/10.1029/92JC00188, 1992.

Webb, J.R., Clough, T.J., Quayle, W.C.: A review of indirect N2O emission factors from artificial agricultural waters, *Environmental Research Letters*, 16 043005, https://doi.org/10.1088/1748-9326/abed00, 2021.

Webb, J.R., Leavitt, P.R., Simpson, G.L., Baulch, H.M., Haig, H.A., Hodder, K.R., and Finlay, K.: Regulation of carbon dioxide and methane in small agricultural reservoirs: optimizing potential for greenhouse gas uptake. *Biogeosciences*, 16 (21), 4211–4227. https://doi.org/10.5194/bg-16-4211-2019, 2019.

Webb, J.R., Quayle, W.C., Ballester, C., Wells, N.: Semi-arid irrigation farm dams are a small source of greenhouse gas emissions. *Biogeochemistry*, 166, 123–138. https://doi.org/10.1007/s10533-023-01100-4, 2023.

Weiss, R. F., Price, B. A.: Nitrous oxide solubility in water and seawater. *Marine chemistry*, *8*(4), 347-359., doi.org/10.1016/0304-4203(80)90024-9, 1980.

Weiss, R. F.: Determinations of carbon dioxide and methane by dual catalyst flame ionization chromatography and nitrous oxide by electron capture chromatography. *Journal of Chromatographic* Science, 19, 611–616. https://doi.org/10.1093/chromsci/19.12.611, 1981.

West, W.E., Coloso, J.J., and Jones, S.E.: Effects of algal and terrestrial carbon on methane production rates and methanogen community structure in a temperate lake sediment. *Freshwater Biology*, 57, 949–955. https://doi.org/10.1111/j.1365-2427.2012.02755.x, 2012.

Wik, M., Crill, P. M., Varner, R. K., and Bastviken, D.: Multiyear measurements of ebullitive methane flux from three subarctic lakes. *Journal of Geophysical Research: Biogeosciences*, 118:791 1307–1321. https://doi.org/10.1002/jgrg.20103, 2013.

Xie, S., T Xia, T., H Li, H., Y Chen, Y., W Zhang, W. , 2024, Variability in N2O emission controls among different ponds within a hilly watershed, *Water Research*, 267, 122467, https://doi.org/10.1016/j.watres.2024.122467, 2024.

Xun, F., Feng, M., Ma, S., Chen, H., Zhang, W., Mao, Z., Zhou, Y., Xiao, Q, Wu, Q. L., and Xing, P.: Methane ebullition fluxes and temperature sensitivity in a shallow lake. *Science of The Total Environment*, *912*, 169589. https://doi.org/10.1016/j.scitotenv.2023.169589, 2024.

928 Yan, X., Xu, X., Ji, M., Zhang, Z., Wang, M., Wu, S., Wang, G., Zhang, C., and Liu, H.: Cyanobacteria blooms: A neglected
929 facilitator of CH4 production in eutrophic lakes. *Science of the total environment*, *651*, 466-474.
930 https://doi.org/10.1016/j.scitotenv.2018.09.197, 2019.

931 Yang, Z., Zhao, Y., and Xia, X.: Nitrous oxide emissions from Phragmites australis-dominated zones in a shallow lake.
932 *Environmental pollution*, *166*, 116-124. https://doi.org/10.1016/j.envpol.2012.03.006, 2012.

933 Yentsch, C.S., and Menzel, D.W.: A method for the determination of phytoplankton chlorophyll and phaeophytin by
934 fluorescence. *Deep Sea Research and Oceanographic Abstracts*, 10. Elsevier, pp. 221–231.
935 https://doi.org/10.1016/0011-7471(63)90358-9, 1963.

936 Zhao, K., Tedford, E.W., Zare, M., and Lawrence, G.A.: Impact of atmospheric pressure variations on methane ebullition
937 and lake turbidity during ice - cover. *Limnology and Oceanography Letters*, 6(5), 253-261.
938 https://doi.org/10.1002/lol2.10201, 2021.

939